People's Democratic Republic of Algeria
Ministry of Higher Education and Scientific Research

University M'Hamed BOUGARA – Boumerdes

Institute of Electrical and Electronic Engineering

Department of Electronics

Final Year Project Report Presented in Partial Fulfilment of the Requirements for the Degree of

'MASTER'

In **Telecommunication**
Option: **Telecommunications**

Title:

Analysis of a Fractal Ultra Wide Band Monopole Antenna with Reconfigurable Notches

Presented By:

- **ABBAD Mohammed**
- **HABTICHE Nabil**

Supervisor:

Dr M. DEHMAS

Registration Number:……/2021

Dedication

We dedicate this work

To our dear parents, who are responsible of who we are
we will be in the future.

To our dear brothers and sister

To all my friends.

ABBAD Mohammed and
habtiche nabil

Acknowledgement

We would like to thank all the people who have assisted me during my graduate school years at the Institute of Electrical and Electronic Engineering, Boumerdes.

We would like to express our sincere gratitude to Mr. M. DEHMAS, our work supervisor, for his support and guidance during my work and report preparation. This work would not have been possible without his continuous help. We also express our gratitude to Pr. A. AZRAR for his help and assistance for the accomplishment of this work. Special thanks go to, Mrs F.MOUHOUCHE, Mrs K.DJAFRI, Dr. M.CHALLAL for their precious help and support in the simulations, implementation and measurements.

Table of Contents

List of figures :

List of tables:

List of Acronyms

BW	Bandwidth
CP	Circular patch
CST	Computer Simulation Technology
EM	Electromagnetic
FR4	Flame Resistant 4
FET	Field effect transistor
GPS	Global Positioning System
GSM	Global System for Mobile Communications
MPA	Microstrip Patch Antenna
PCB	Printed Circuit Board
RE-MEMs	Radio-Frequency micro-electromechanical systems
RF	Radio frequency
RFID	Radio Frequency Identification
UWB	Ultra Wide Band
VSWR	Voltage Standing Wave Ratio
WiMax	Worldwide Interoperability for Microwave Access
WLAN	Wireless Local Area Network

ABSTRACT

This work describes the design and analysis of a fractal Ultra-Wide Band (UWB) coplanar fractal antenna with triple reconfigurable notch rejection bands. The investigation considers three successive configurations: coplanar monopole circular UWB antenna – Fractal coplanar monopole UWB band antenna with improved bandwidth – Slotted UWB structure with reconfigurable notches. Reconfigurability is achieved by opening / short-circuiting appropriate slots to select the rejected band(s).

This study has ended with three reconfigurable notches bands covering the frequency bands: $[4.50\ GHz, 5.35\ GHz]$, $[6.30\ GHz, 7.15\ GHz]$ and $[8.15\ GHz, 8.60\ GHz]$ including Wi-Max and WLAN applications and X band.

The developed structure was printed on a 21x25x1.63 mm^3 glass epoxy FR-4 substrate. The input reflection coefficient has been measured where an agreement was observed between simulated and experimental results.

The simulations concerning the input reflection coefficients, current distributions and radiation patterns were carried out using the CST Microwave Studio.

Introduction

Flexible, small and high efficiency antennas become very necessary in nowadays technology. Microstrip Patch Antennas fit those criterions as they have contributed in several solutions for many systems requirements and radiating elements. It is a very common element in nowadays telecommunication applications for providing a variety of designs. [1-2]

Recently, the use of Microstrip Patch antennas has grown due to their advantages. However, research is still on and several improvements have been achieved in wireless telecommunication systems.[3-4]

This project deals with design, analysis, fabrication and testing of an UWB Fractal Microstrip Patch antenna with reconfigurable notches. The achieved work, inspired from [5], presents improvement in bandwidth and a qualitative radiation pattern.

This report includes three main chapters organized as follow:

- **Chapter one:** It presents an overview on microstrip patch antennas including a general description, feeding techniques, advantages/disadvantages, applications as well as the method of analysis of these antennas. Also, it provides basic theory about reconfigurable antennas including their types and techniques.

- **Chapter two:** This chapter deals with the design and analysis of a Fractal Ultra-Wide Band Patch Antenna. The design method and parameters of the fractal antenna and the simulated results of the antenna.

- **Chapter three:** This part describes the performed modifications on the above structures by adding a U-shaped slot on the patch and an L-shaped slot on the ground plane along with switches. It shows how those slots act on rejecting frequencies bands. The structure has been fabricated and tested where the experimental results have been compared to the simulated ones.

Finally, it ends up with a general conclusion where suggestions for further scope are given.

Chapter 1

Generalities on Microstrip Antennas and Reconfigurability

1.1 Introduction

An antenna, known as transducer, is an interface for energy traveling between a circuit and free space. In other words, antennas are interfaces between radio waves propagating through space and electric currents moving in metal conductor.

Antennas can be used with a transmitter or receiver. In transmission, a radio transmitter circuit supplies an electric current to the antenna's terminal and the antenna radiates the energy from the current source as radio waves. In reception, an antenna acts as a source by intercepting some of the power of a radio wave in order to produce and electric current at its terminals. The current is then applied to a receiver circuit to be amplified.

Antennas can be designed to transmit and receive radio waves in all horizontal directions equally, also called omnidirectional antennas, or preferentially in a particular direction in case of directional antennas.

The concept of microstrip antenna was first introduced in the 1950s. It had to wait until the development of Printed Circuit Board (PCB) technology in 1970s to be realized. Since then, microstrip antennas are the most commonly used antennas with a wide range of applications due to their apparent advantages. They have been widely engaged for the civilian and military application (such as Radio Frequency Identification, RFID), radio broadcast, mobile systems, Global Positioning System (GPS), television, satellite communications, radar systems and remote sensing [6].

A Microstrip or Patch antenna is a single-layer design which consists generally of four parts labeled as patch, ground plane, substrate and the feeding part as illustrated in Figure (1.1) [6]

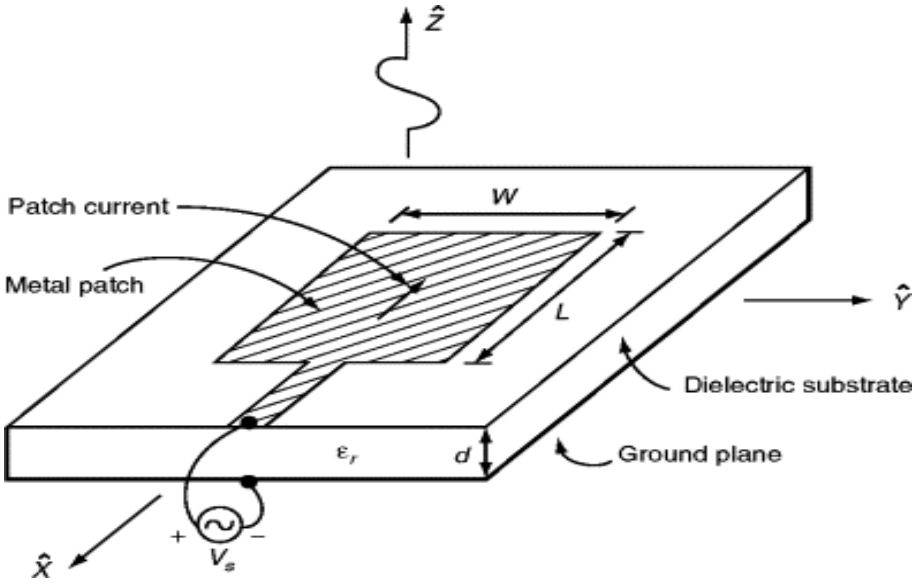

Figure 1.1 Geometry of a Rectangular Microstrip Antenna

1.1.1 Types of Patch Antennas

There exists several shapes of microstrip antennas. They have been designed to meet specific characteristics. Some of the common types are shown in **Figure 1.2 [6]**. Rectangular, square and circular patches are commonly used for millimeter wave frequencies.

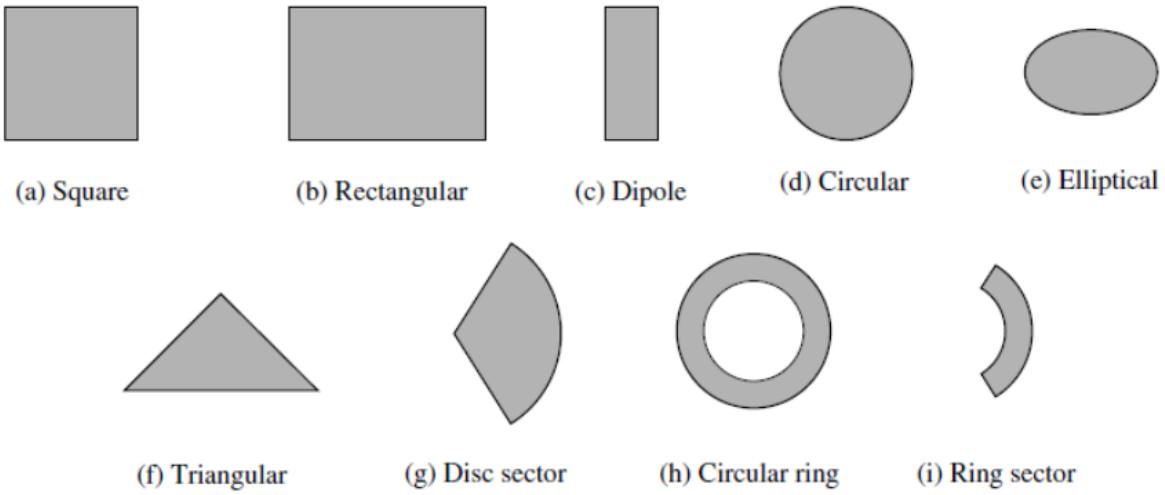

Figure 1.2: Types of microstrip antennas

Choose of the substrate is also crucial. Temperature, humidity and other environmental ranges of operating have to be considered. Thickness of the substrate h has a big effect on the resonant frequency f_r and bandwidth BW of the antenna. BW is directly proportional to the thickness h but with limits. Otherwise, the antenna will stop resonating.

1.1.2 Feeding Techniques

Different methods are available to feed microstrip patch antennas. These methods can be contacting and non-contacting methods. There are many feeding techniques but the four most popular used are: microstrip line, coaxial probe (both contacting schemes), aperture coupling and proximity coupling (both non-contacting schemes) [7].

a- Coaxial Feed

A coaxial feed technique is shown in **Figure 1.3 [7]**. The inner conductor of the coaxial connector extends throughout the substrate and is soldered to the radiating patch while the outer conductor is soldered to the ground plane. The major advantage of this is that the feed can be placed at any desired location inside the patch in order to match with its input impedance. The disadvantage, however, is that it provides narrow bandwidth and is complex to model.

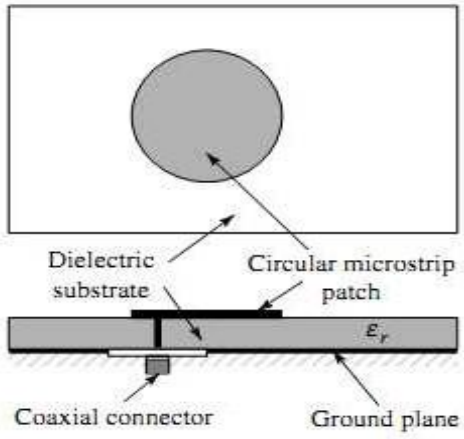

Figure 1.3 Coaxial feed technique

b- Microstrip Line Feed

A conducting strip is connected directly to the edge of the microstrip patch. The conducting strip is smaller in width as compared to the patch as shown in **Figure 1.4 [7]**. This kind of feed arrangement has the advantage that the feed can be etched on the same substrate to provide a planar structure.

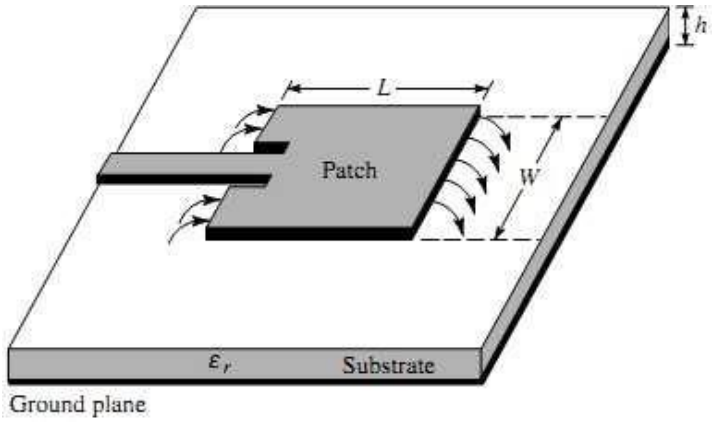

Figure 1.4 Microstrip line feed

c- Aperture Coupled Feed

The radiating patch and the microstrip feed line are separated by the ground plane as illustrated in **Figure 1.7**. The patch and the feed line are coupled through a slot in the ground plane. The coupling slot is centered below the patch, leading to low cross polarization due to symmetry of the configuration.

Since the ground plane separates the patch and the feed line, spurious radiation is minimized. However, the main disadvantage of this feed technique is that it is difficult to implement due to multiple layers, which also increases the antenna thickness.

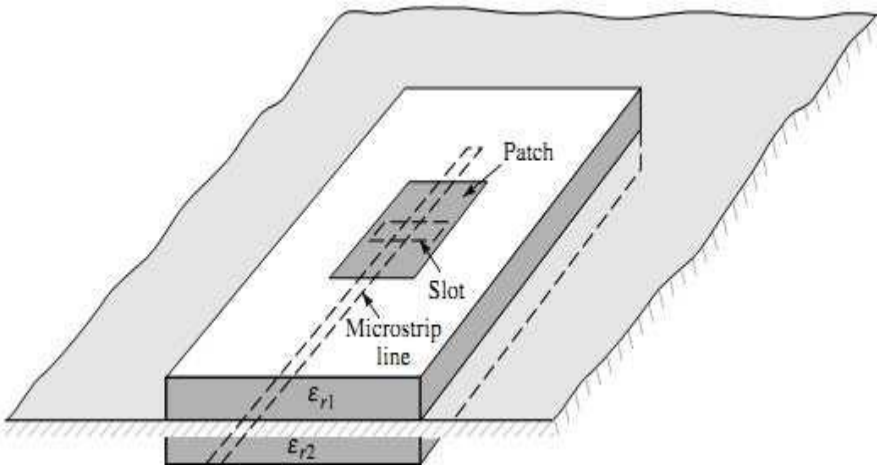

Figure 1.5 Aperture coupled feed

d- Proximity Coupled Feed (Electromagnetic Coupling Scheme)

This technique is shown in **Figure 1.6 [7].** Two dielectric substrates are used and the feed line is between the two substrates. The radiating patch is on top of the upper substrate.

The advantage of this feed technique is that it eliminates spurious feed radiation and provides very high bandwidth (as high as 13%). On the other hand, it is difficult to fabricate because of the two dielectric layers which need proper alignment.

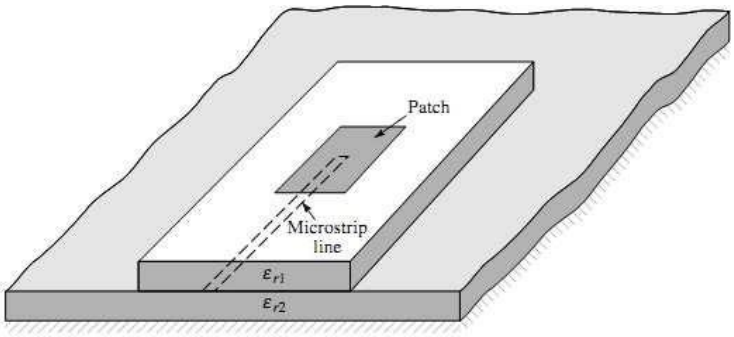

Figure 1.6 Proximity coupled feed

1.1.3 Characteristics of Patch Antennas:

Important parameters have to be considered before designing microstrip antennas, which are the frequency, bandwidth, gain, impedance and polarization. Some fundamental parameters will be introduced in this section.

a- Input Impedance

The impedance presented by an antenna at its terminal, in other words the ratio of the voltage to the current at the pair of terminals, is called the input impedance. It can also be defined as the ratio of the appropriate components of the electric to the magnetic fields at a point. The input impedance Z_{in} can be represented in its complex form as shown in eq (1.1).

$$Z_{in} = R_{in} + jX_{in} \qquad (1.1)$$

where:

R_{in} is the input resistance

X_{in} is the input reactance

b- Input reflection coefficient

Input reflection coefficient (S11 or Γ) is related to the input impedance and the maximum transfer of power theory. It is defined as the power reflected back from the antenna P_r to the source incident power of the antenna P_i as shown in eq (1.2)

$$|S11|(dB) = 10\log\left(\frac{P_r}{P_i}\right) = 20\log|\Gamma| = 20\log\left(\frac{|Z_{in}-Z_0|}{|Z_{in}+Z_0|}\right) \quad (dB) \qquad (1.2)$$

Where:

Z_{in} is the input impedance of the antenna.

Z_0 in the characteristic impedance ofthe feed line.

c- Voltage Standing Wave Ratio (VSWR)

VSWR represents the ratio of the maximum voltage to the minimum and it is always greater than one.It is given by equation (eq 1.3) below.

$$VSWR = \frac{1 + |\Gamma|}{1 - |\Gamma|} \tag{1.3}$$

Where Γ is the reflection coefficient defined as $\Gamma = \frac{V_r}{V_f}$. V_f is the complex amplitude of the forward wave and V_r is the complex amplitude of the reflected wave.

The impedance of a particular antenna design can vary due to a numerous factors that cannot always be clearly identified. This includes the transmitter frequency (as compared to the antenna's design or resonant frequency), the antenna's height above the ground and proximity to large metal structures, and variations in the size of the conductors used to construct it (3).

d- Frequency Bandwidth BW

It is defined as "The range of usable frequencies within which the performance of the antenna, with respect to some characteristic, conforms to a specified standard" as it is shown in **Figure 1.7**.

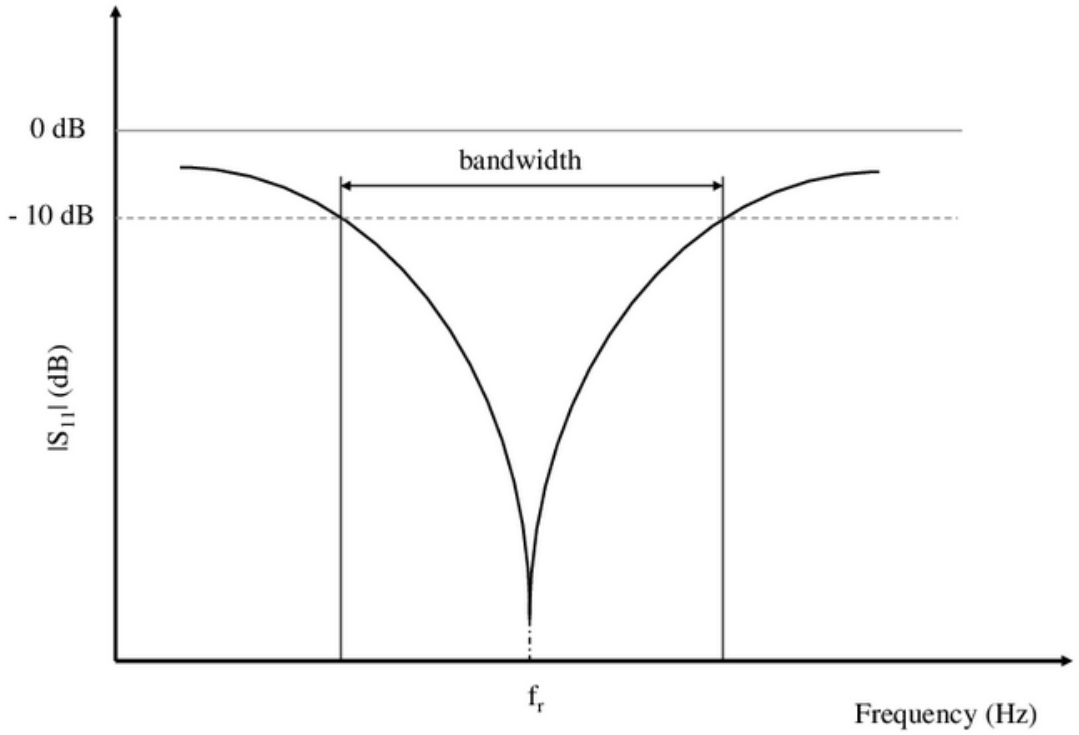

Figure 1.7 Bandwidth of an antenna

It is generally defined as the range of frequencies where

$$|S11|\text{dB} \leq -10 \text{ dB} \qquad (1.4)$$

Where S11= |Γ|

It is sometimes defined as the frequency band where the VSWR is within the range

$$1 \leq VSWR \leq 2 \qquad (1.5)$$

Important Note:

From eq. (1.3) above, VSWR = 2 yields $|S11|$dB = - 9.33 dB. Consequently, the estimated bandwidth based on eq. (1.5) is larger than the one based on eq. (1.4).

Another parameter, usually used to evaluate the Ultra Wide Band Antenna performance, is the percent bandwidth (%BW) estimated as:

$$\%BW = \frac{fh - fl}{fh + fl} \times 200\% \qquad (1.6)$$

where *fh* and *fl* are respectively the upper and the lower operating frequencies of the antenna.

e- Radiation Pattern

Radiation pattern is mathematical or graphical model that represents the radiation properties of an antenna as a function of space coordinates. Radiation properties include power flux density, radiation intensity, field strength, directivity phase and polarization. Commonly, the radiation pattern is determined only in the far region and is represented as function of directional coordinates.

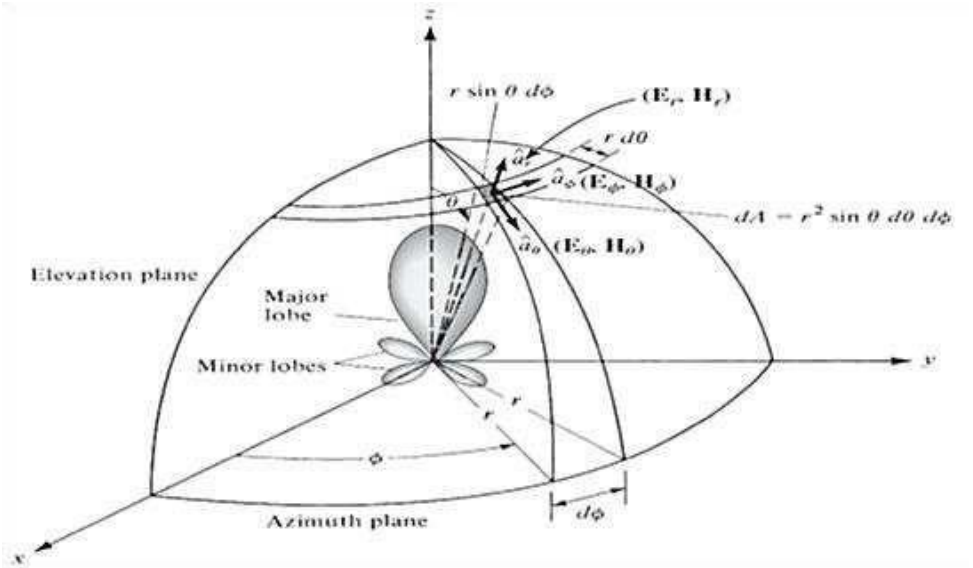

Figure 1.8 Coordinate System for Antenna Analysis [**2**]

f- Directivity

Directivity defines the ratio of the radiation intensity in a given direction from the antenna to the radiation intensity averaged over all directions. It measures the degree to which the radiation emitted is concentrated in a single direction.

$$D = \frac{U}{U_0} = \frac{4\pi U}{P_{rad}} \qquad (1.7)$$

The maximum directivity is given by

$$D_{max} = D_0 = \frac{U_{max}}{U_0} = \frac{4\pi U_{max}}{P_{rad}} \qquad (1.8)$$

Where:

U_0 is the average radiation intensisty

U, U_{max} are the radiation intensity and the maximum radiation intensity, respectively.

P_{rad} is the power radiated

g- Gain

The gain of an antenna is defined as the ratio of the power intensity radiated by the antenna in a given direction to the power intensity radiated by a lossless isotropic antenna, which radiates the power at all angles equally. It is usually given in spherical coordinate angles θ and φ and can be formulated as:

$$Gain = G(\theta, \varphi) = 4\pi \frac{U(\theta,\varphi)}{P_{in}} = e.D \qquad (1.9)$$

Where $e = \frac{P_{rad}}{P_{in}}$

e: efficiency

h- Beamwidth

"In a plane containing the direction of the maximumof a beam, the angle between the two directions in which the radiation intensity is one half themaximum value of the beam**"** [7] [8]

The $-3dB$ beamwidth may be calculated from the radiation pattern in both principal planes. These values can be more explored to calculate the maximum directivity as:

$$D = 10 \log\left(\frac{26000}{\theta_E \theta_H}\right) \quad (dB) \qquad (1.10)$$

Where θ_E and θ_H are respectively the beamwidth in the principal planes.

1.1.4 Application of Microstrip Antennas

Microstrip antennas have applications in several fields. They are booming in the commercial aspects due to their low cost of the substrate material and the fabrication. Some of these applications are listed below:

- Mobile and satellite communications.
- Radio Frequency Identification (RFID)
- Radar application
- WLAN applications
- GPS application

Table 1.1 below lists some microstrip antennas applications and their frequencies.[8]

Table 1.1 Applications of Some Microstrip Patch Antennas and their Frequencies.

Application	**Frequency**
Global Positioning Satellite	1575 MHz and 1227 MHz
Cellular Phone	824-849 MHz and 869-895 MHz
Personal Communication Systems	1.85-1.99 GHz and 2.18-2.20 GHz
GSM	890-915 MHz and 935-960 MHz
Wireless Local Area Network	2.40-2.48 GHz and 5.4 GHz
Direct Broadcast Satellite	11.7-12.5 GHZ
Automatic Toll Collection	905 MHz and 5-6 GHz
Cellular Video	28 GHz
Collision Avoidance Radar	60 GHz, 77 GHz and 94 GHz
Wide Area Computer Network	60 GHz

1.1.5 Advantages and Disadvantages of Microstrip Antenna:

Some advantages of patch antennas [8] are listed below:

- Lightweight and low volume
- Low fabrication cost, hence large quantity manufacturing.
- Ease of integration with microwave integrated circuits.
- Low profile planar configuration.
- Supporting both linear and circular polarization.
- Capability of dual and triple frequency operations.

However, as all other technologies, patch antennas have disadvantages [8] some of them can be seen below:

- Low efficiency
- Narrow bandwidth
- Low gain
- Surface wave excitation
- Low power handling capacity.

The antenna bandwidth can be extended by incorporating parasitic elements, using high permittivity substrate, creation of multiple resonances and/or by using fractal shapes.

1.2 Reconfigurable Antennas

A reconfigurable antenna is an antenna that is able to modify its parameters as frequency, polarization and radiation pattern dynamically in a controlled and reversible manner [8]. To provide a dynamic response, reconfigurable antennas integrate an inner mechanism, such as RF switches, PIN diodes, varactors, mechanical actuators that enable the intentional redistribution of the RF currents over the antenna surface and produce reversible modifications of its properties.

1.2.1 Types of Antenna Reconfiguration

Depending on the dynamically adjusted parameter, reconfigurable antennas can be classified. Typically, those parameters are the frequency of operation, radiation pattern and polarization [8].

a- Frequency Reconfiguration

In this class, the frequency can be dynamically adjusted. The use of this technique can be seen in situations where several communication systems converge because the multiple antennas can be replaced by a single reconfigurable antenna. The frequency reconfiguration can be achieved by physical or electrical modification to the antenna using RF switches, impedance loading or tunable materials [8-9-10]

b- Radiation Pattern Reconfiguration

Reconfigurability of radiation pattern is based on the intentional modification of the spherical distribution of the radiation pattern. Beam steering is the most extended application and consists of steering the direction of maximum radiation to maximize the antenna gain in a link with mobile devices. They are usually designed using movable or rotatable structure or switchable and reactively loaded parasitic elements [10-13].

c- Polarization Reconfiguration

These types of antennas are capable of switching between different polarizations modes. The capability of switching between horizontal, vertical and circular polarizations is used to reduce polarization mismatch losses in portable devices. These reconfigurations can be provided by changing the balance between the different modes in a multimode structure.[14]

1.2.2 Reconfiguration Techniques

Several reconfiguration techniques exists for antennas. Mainly they are electrical [15], optical, physical (mechanical) [16] and using materials. For this last one, the material can be solid, liquid crystal or liquids (21).The reconfiguration techniques are presented in **Figure 1.9**.

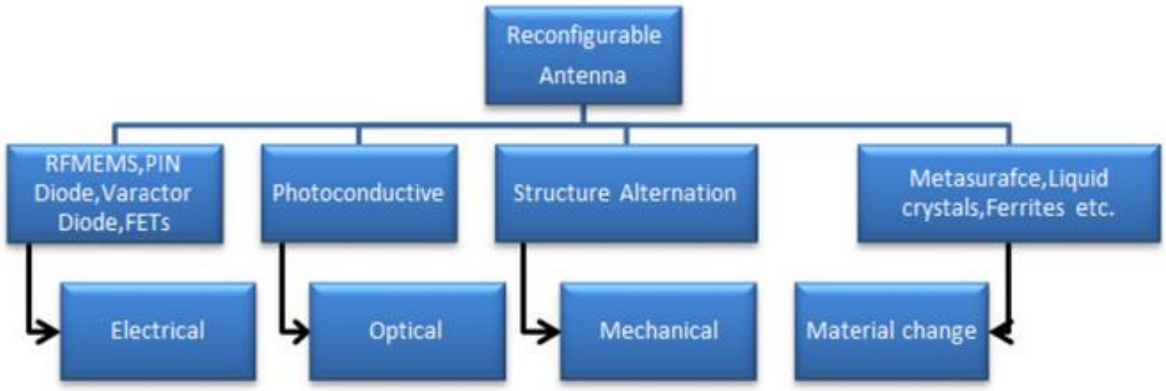

Figure 1.9 Schematic of reconfigurable techniques.

a- Electrically Reconfigurable Antennas

Electronic components are used in this technique. Mainly, they are Radio-Frequency micro-electromechanical systems (RE-MEMs), PIN diodes, varactors or FET transistors. They are used for surface current distribution by altering the antenna radiating structures.

b- Optically Reconfigurable Antenna

Resonant Frequency of an antenna can also be achieved by optically controlled switches. Optically reconfigurable antennas come under the class of radiating elements that have the capability of changing the radiation properties with the use of switches which may be optical activation of silicon switches of reactive elements [3].

c- Mechanically or Physically Reconfigurable Antennas

The antenna radiating structure can be physically altered to configure it. The tuning of the antenna is achieved by a structural modification of the antenna radiating parts [17-18]. The importance of this technique is that it does not rely on any switch mechanisms, biasing lines

or optical fiber/laser diode integration.

d- Smart Materials Based Reconfigurable Antenna

The substrate characteristics can be changed to reconfigure the antenna. Indeed, materials as liquid crystals, dielectric fluids, ferrites or metamaterials can be incorporated to the substrate to change its characteristics. This change is achieved by a change in the relative electric permittivity ε_r or magnetic permeabilityμ_r.

1.4 Conclusion

In this chapter, we covered some important points about microstrip patch antennas, basic characteristics, and fundamental parameters as we went through their techniques of analysis. After that, we moved to reconfigurable antennas structures that have specific abilities to modify parameters as frequency, polarization and radiation pattern dynamically.

Chapter 2

Fractal Ultra-Wide Band Patch Antennas Design and Analysis

In this chapter, a fractal ultra-wide band patch antenna fed by a microstrip line is obtained and discussed. In the next chapter, reconfigurable notches will be introduced to this UWB structure. This work is inspired from a work published in 2019 [5] to which an improvement is provided mainly to the operating bandwidth.

In the first step of this part., an UWB circular disk patch antenna is considered. In the second step, two successive fractal iterations are performed and which resulted in a wider operating bandwidth.

The simulated structures return loss, input impedance, current distribution and radiation patterns obtained using CST Microwave Studio Simulator are illustrated.

Note: Several physical parameters and dimensions of the original antenna are missing in [5**]**.We have then unsuccessfully contacted the author in order to get them. After that, simulations dealing with many physical and geometrical parameters are performed throughout all this work after which appropriate dimensions fitting the objectives related to the operating bandwidth and to the reconfigurable notches are obtained.

2.1Original Circular Disk Patch Antenna

2.1.1Antenna Geometry

The considered original UWB circular disk monopole planar patch antenna is shown in **Figure 2.1.**

As illustrated in this figure, the original (0^{th} iteration) UWB structure consists of a circular patch feed by a stripline with a coplanar ground. The patch is mounted on the FR-4 dielectric material substrate with a relative permittivity of 4.3, a loss tangent of 0.017 and a thickness of 1.63 mm. The obtained geometrical dimensions are illustrated in **Table 2.1**.

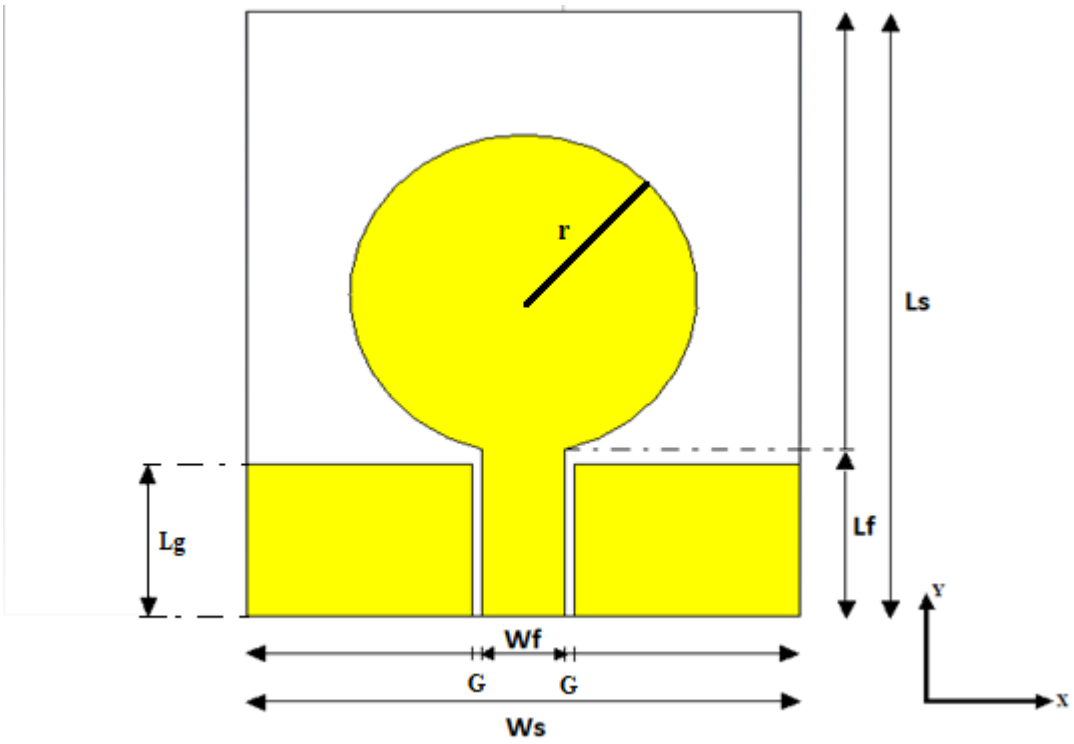

Figure 2.1 Original circular disk patch antenna

Table 2.1 Schematic Parameters of the Microstrip Patch Antenna

Symbol	Description	Value (mm)
L_S	Substrate length	**25**
W_S	Substrate width	**21**
Lg	Ground plane length	**5.8**
r	Circular patch radius	**6.8**
G	Feed line–Ground plane gap	**0.36**
Lf	Feed line length	**6.5**
Wf	Feed line width	**3.124**

2.1.2 Input reflection coefficient

The performed simulations with variation of geometrical dimensions mainly the feed line–ground plane gap, the feed line width and length to achieve a good power matching has led to the input reflection coefficient graph shown in **Figure 2.2**.

This figure shows that the antenna operating bandwidth extends from 4.12 GHz to 9.71 GHz corresponding to a %BW of 80.84%.

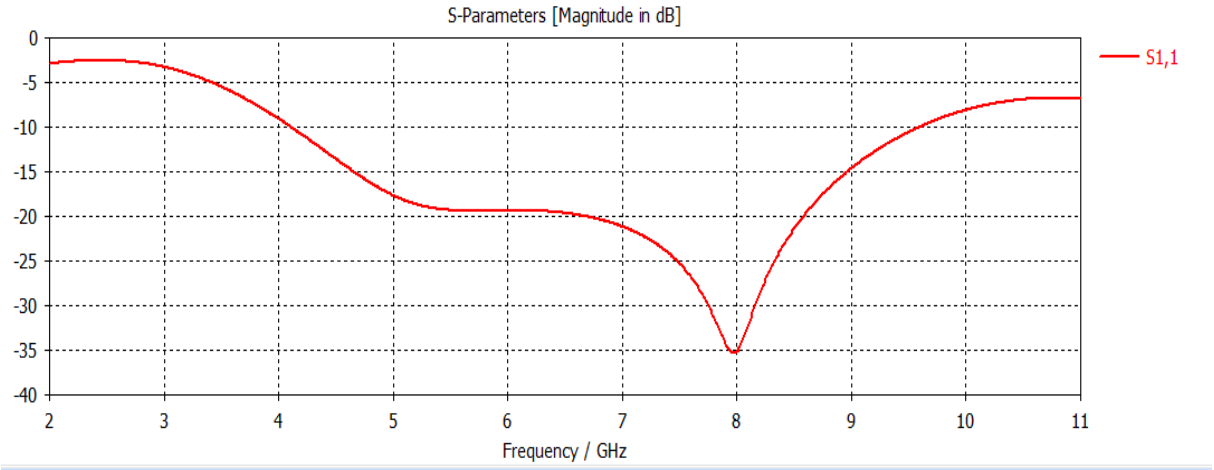

Figure 2.2 Original Antenna input reflection coefficient

2.2 Fractal shape monopole antenna

2.2.1 Design Procedure

In order to enhance the original structure operating bandwidth, two successive iterations of a fractal shape is introduced on the patch.

In each iteration, a new circular shape of radius *r* centered at a distance s from the center of the previous circular shape(s). The fractal shapes and details for iteration 1 and 2 successively are shown in **Figure 2.3** and **Table 2.2.**

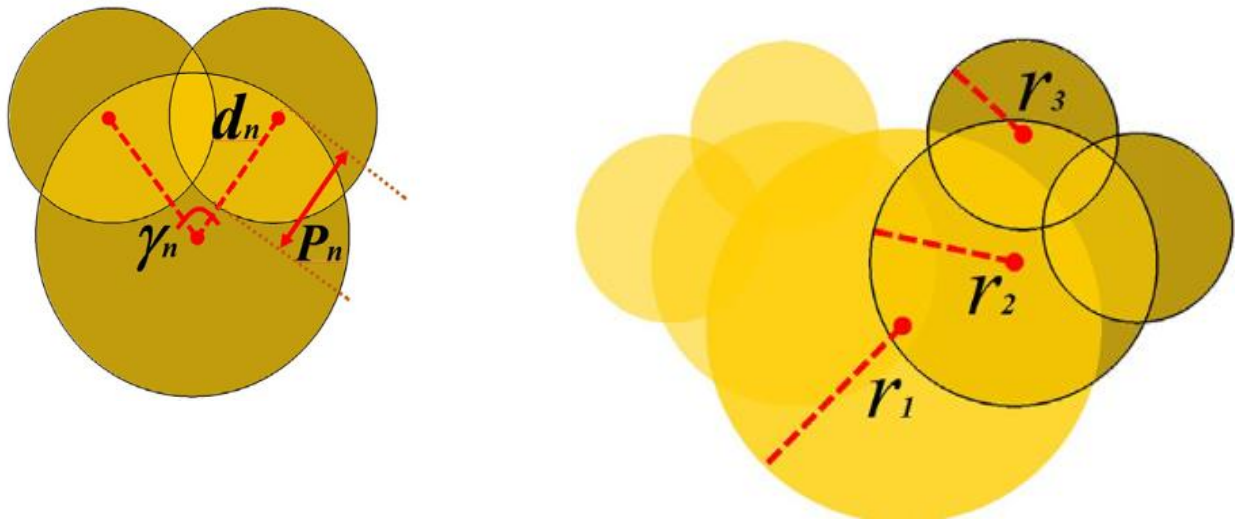

(a) **(b)**

Figure 2.3 Fractal Shapes **(a)** First iteration and, **(b)** Second iteration (final patch shape)

The geometrical dimensions at the n^{th} iteration are determined by using the relation below describing the used fractal procedure [5]:

$$(r_n = a_n \times r_{n-1}). \tag{2.1}$$

$$D_n = \frac{p_n}{r_n + r_{n-1}} = \frac{r_n + r_{n-1} - d_n}{r_n + r_{n-1}} = 1 - \frac{d_n}{r_n + r_{n-1}} = 1 - \frac{1}{1 + a_n} \cdot \frac{d_n}{r_{n-1}} \tag{2.2}$$

where the different parameters are illustrated in **Figure 2.3** and their values shown in **Table 2.1.**

Table 2.2 Patch dimensions

Parameter	Value	Parameter	Value
r1	6.6 mm	D1	0.6
r2	5.8 mm	D2	0.6
r3	3.9 mm	P1	0.6
ɤ	60°	P2	0.6

2.2.2 Simulated input reflection coefficient

a. First iteration

The antenna shape after the first iteration takes the form if **Figure 2.4**. The dimensions are illustrated of **Table 2.1**.

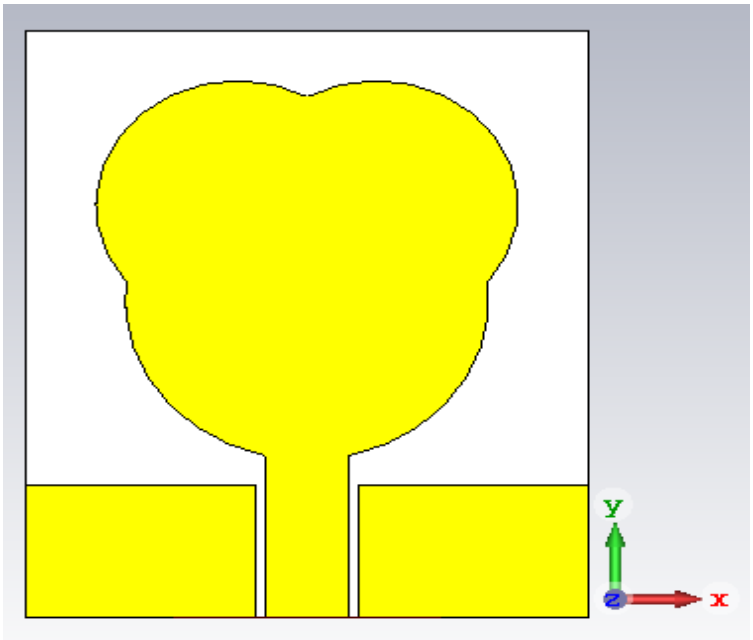

Figure 2.4 Antenna structure after the first iteration

The simulated input refection coefficient is illustrated in **Figure 2.5**.

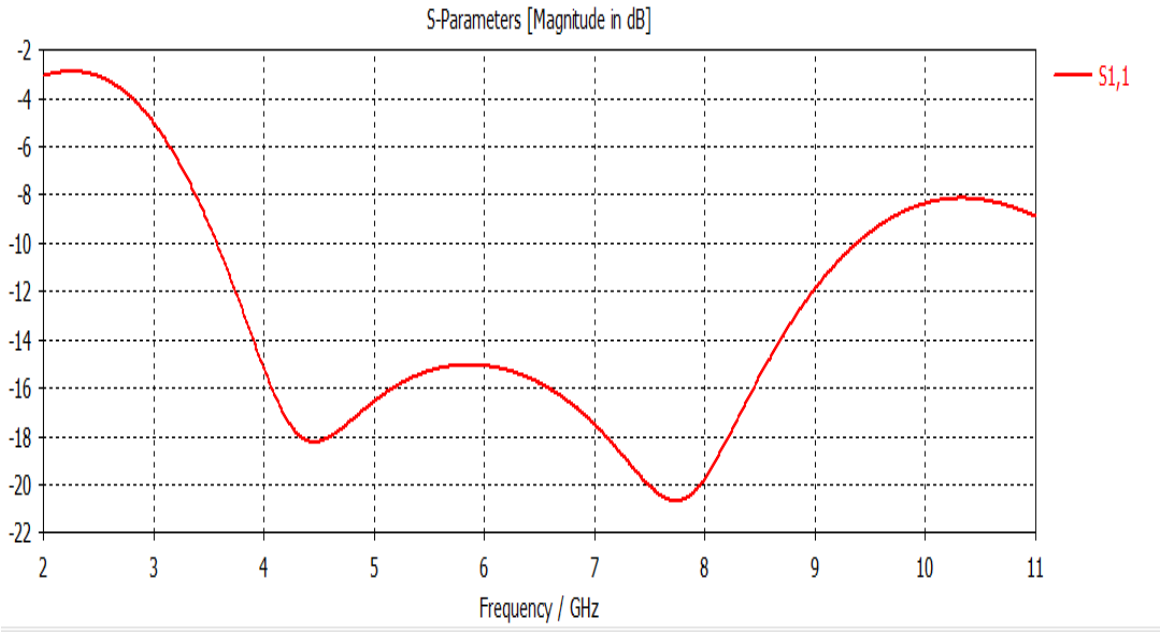

Figure 2.5 Input reflection coefficient after the first iteration.

This figure shows that the antenna operating bandwidth extends from 3.85 GHz to 9.55 GHz corresponding to a % BW of 86.07%.

b. Second iteration

The antenna shape after the second iteration takes the form of **Figure 2.6**. Again, the dimensions are illustrated in **Table 2.1** .

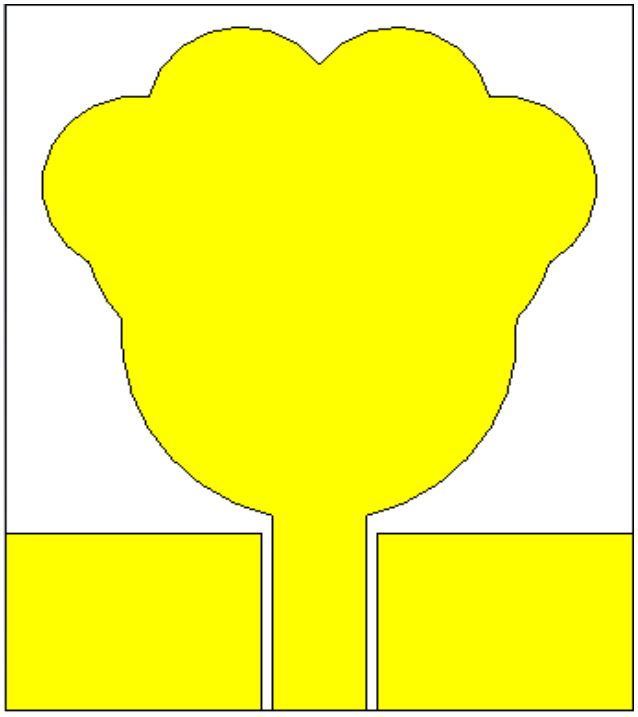

Figure 2.6 Antenna structure after the second iteration.

The simulated input refection coefficient is illustrated in **Figure 2.7**.

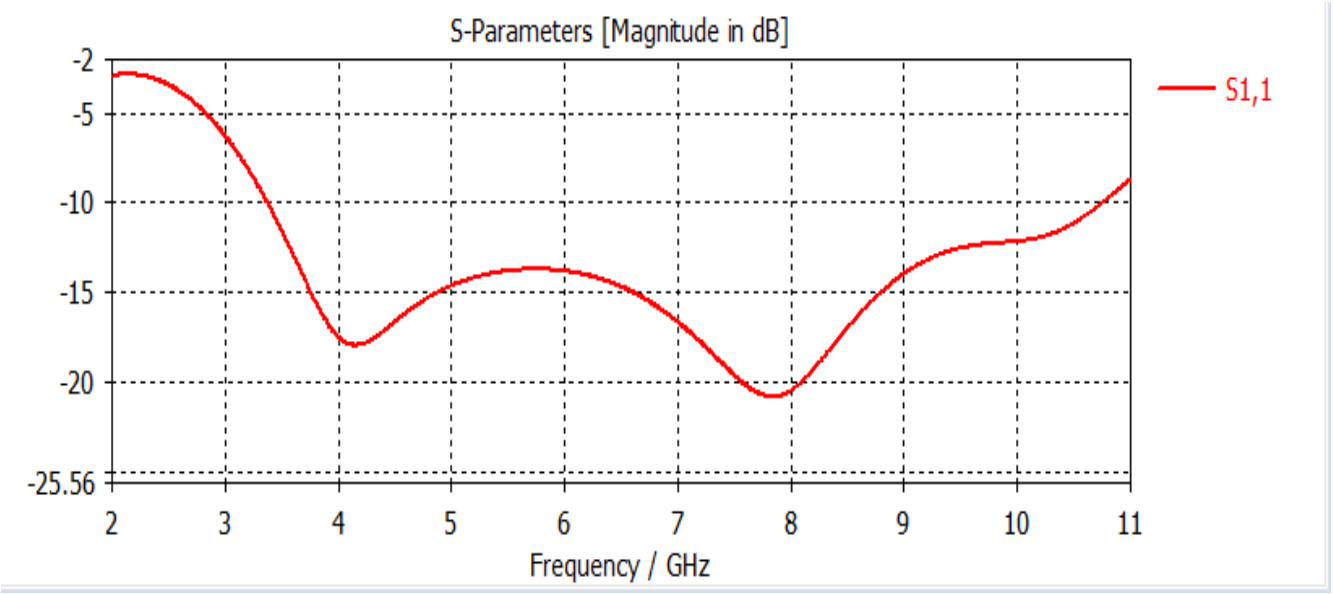

Figure 2.7 Input reflection coefficient of the antenna after the second iteration.

This figure shows that the antenna operating bandwidth extends from 3.32 GHz to 10.79 GHz corresponding to a % BW of 105.88% which provides an improvement with respect to the previous structure.

2.2.3 Bandwidth Characteristics

A comparison between the investigated antennas bandwidth characteristics is summarized in **Table 2.3**. It is observed that the operating bandwidth has been improved in the fractal shaped antennas. Indeed, in the original (0^{th} iteration) circular disk antenna, the operating band based on the $|S_{11}|$ dB $\leq$ -10 dB criterion extends from 4.12 GHz to 9.71 GHz. By adding the lobes at the first iteration, the band has been improved to [3.85 –9.55 GHz]. A further significant improvement is obtained at the second iteration with an operating band of [3.32 –10.79 GHz] which corresponds to a %BW of 105.88%.

Furthermore, in order to compare the obtained antenna operating bandwidth with that of the structure in [5], and since the former one has been estimated based on the VSWR criterion ($\leq$2), the table below provides also a comparison based on this criterion. In this sense, it is noticed that developed antenna presents a wider bandwidth and %BW.

Table 2.3 Band Characteristics

Structure	Bandwidth [GHz]		% BW (%)	
	$\|S_{11}\|$ dB ≤ -10	VSWR≤2	$\|S_{11}\|$ dB ≤-10	VSWR≤2
Original (0^{th} iteration)	[4.12 –9.71]	[4.07 –9.73]	80.84	82.03
First iteration	[3.85 –9.55]	[3.80 – 9.59]	86.07	86.48
Second iteration	[3.32 –10.79]	[3.28 –10.82]	105,88	106.95
Antenna in [5]	--------	[3.1 –10]	--------	105.34

2.2.4 Current density and radiation pattern

The current density distribution and the radiation pattern of the obtained UWB antenna are simulated at three different frequencies. These frequencies are selected at the lower, middle and higher parts of the operating bandwidth. They are 3.45 GHz, 5.2 GHz and 8.1 GHz which correspond to are respectively to WIMAX, WLAN and within X band applications.

a. At 3.45 GHz

- **Current density distribution**

Figure 2.8 illustrates the simulated surface current distribution on the antenna at 3.45 GHz. It is observed from this figure that the maximum current density occurs at the feed line and in the bottom of the circular patch then start decreasing gradually when moving far from it. Moreover, the current density is much stronger at the bottom and lower edges of the circular patch and starts decreasing at the upper edges.

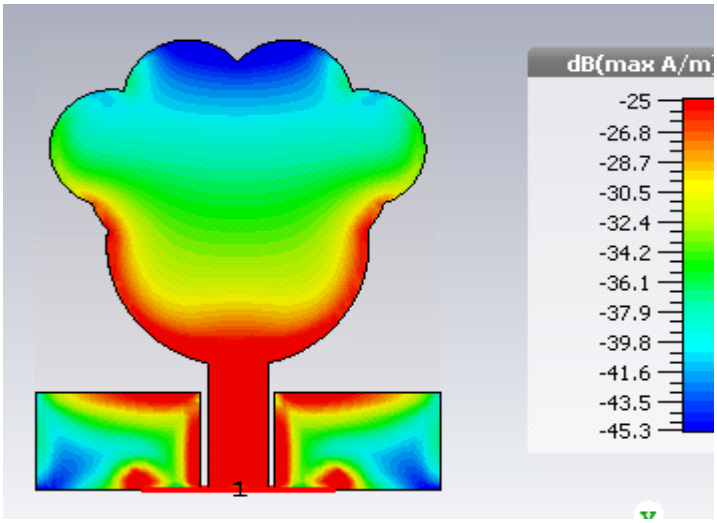

Figure 2.8 Current density distribution at 3.45 GHz

- **Radiation pattern**

Figures 2.9 and **2.10** show the 2D farfield radiation patterns at the frequency 3.45 GHz in

the E- (φ=90°) and H- (φ=0°) planes respectively.

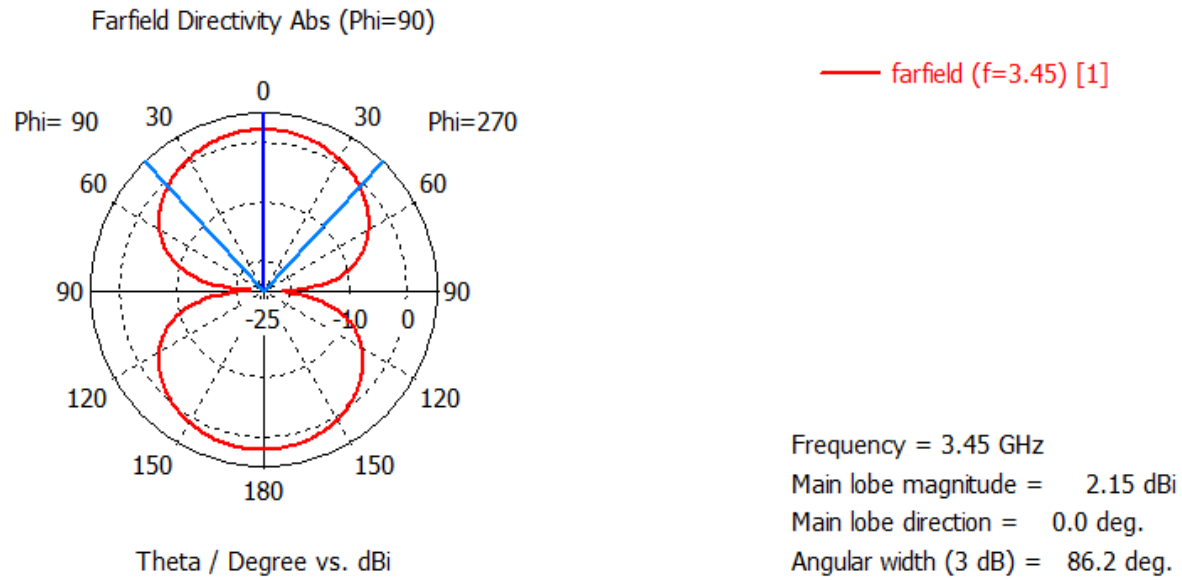

Figure 2.9 Radiation pattern in E-plane at 3.45 GHz

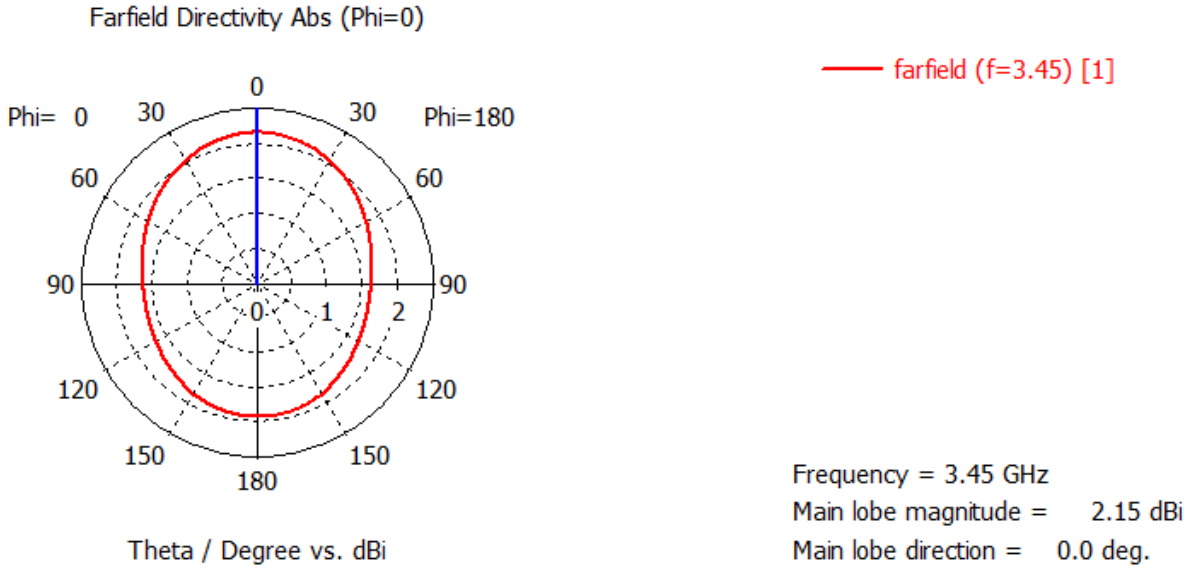

Figure 2.10 Radiation pattern in H-plane at 3.45 GHz

Figure 2.9 shows two lobes in the E-plane, one in the lower and one in the upper hemisphere with a maximum directivity of 2.15 dBi in the direction θ=0°.

Figure 2.10 indicates an almost omnidirectional pattern in the H-plane with a slightly higher directivity of 2.15 dBi in the *z*-direction.

b. At 5.2 GHZ

- **Current density distribution**

Figure 2.11 illustrates the simulated surface current distribution on the antenna at 5.2 GHz.

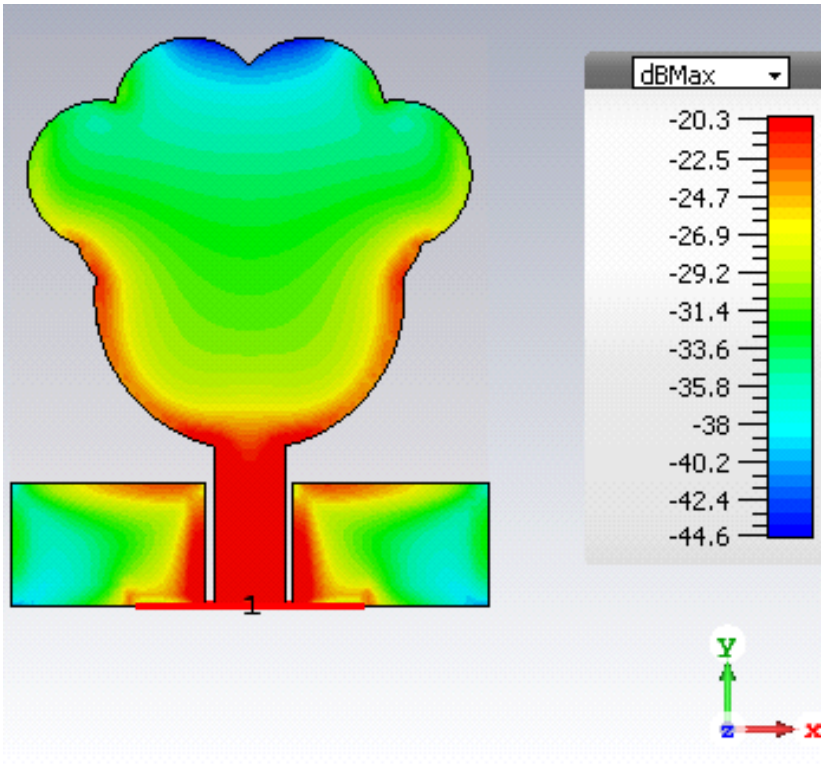

Figure 2.11 Current density distribution at 5.2 GHz

It is observed that the maximum surface current density occurs at the feed line and decreases gradually when moving far from it. Moreover, the current density is much stronger at the lower edges of the iterated circular patch and start decreases at the lateral edges.

- **Radiation pattern**

Figures 2.12 and **2.13** illustrate the 2D farfield radiation patterns at the frequency 5.2 GHz in the E- (φ=90°) and H- (φ=0°) planes respectively.

Again, and as expected from a coplanar structure, **Figure 2.12** shows that radiation occurs in both hemispheres with two lobes. The main lobe exhibits a maximum directivity of 2.78 dBi in the direction θ=172°.

Similarly, **Figure 2.13** shows two lobes in the H-plane, one in the upper and one in the lower hemisphere, with a maximum directivity of 2.66 dBi in the direction θ=180°.

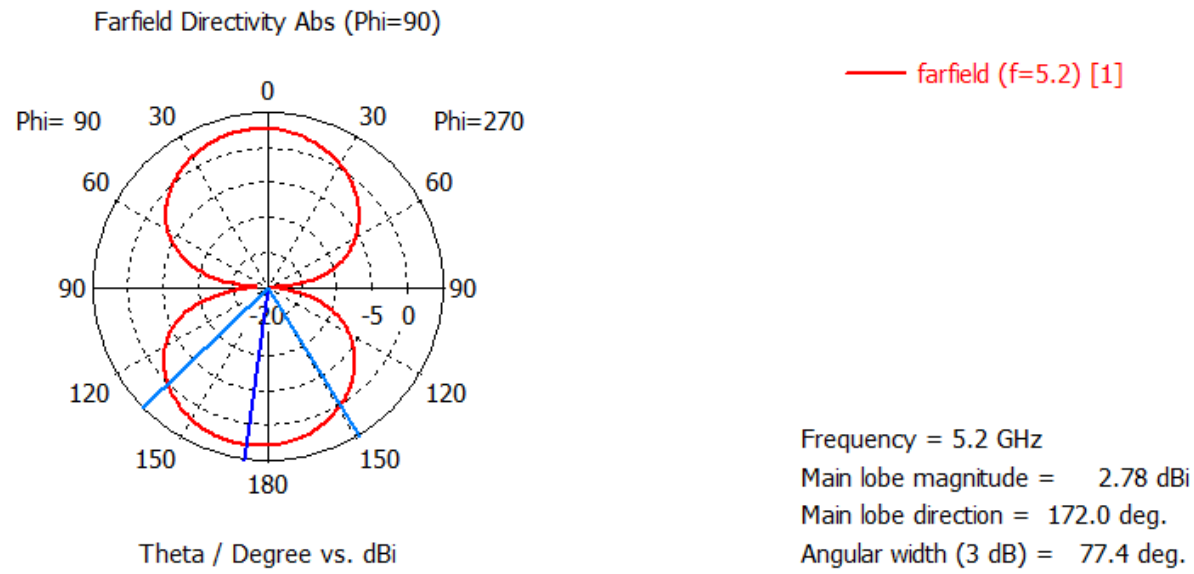

Figure 2.12 Radiation pattern in E-plane at 5.2 GHz

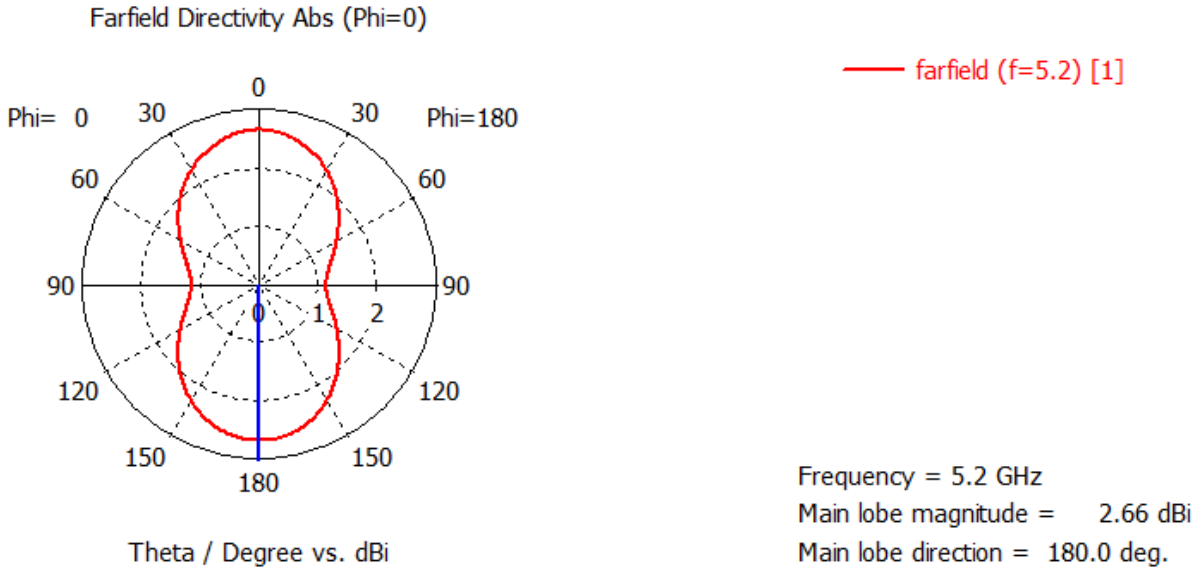

Figure 2.13 Radiation pattern in H-plane at 5.2 GHz

c. At 8.1 GHz

- **Current density distribution**

Figure 2.14 illustrates the simulated surface current distribution on the antenna at 8.1 GHz.

It is observed that the maximum current density level occurs at the feed line and starts decreases when moving far from it. Moreover, the current density is weak in the center and in the top area of the patch.

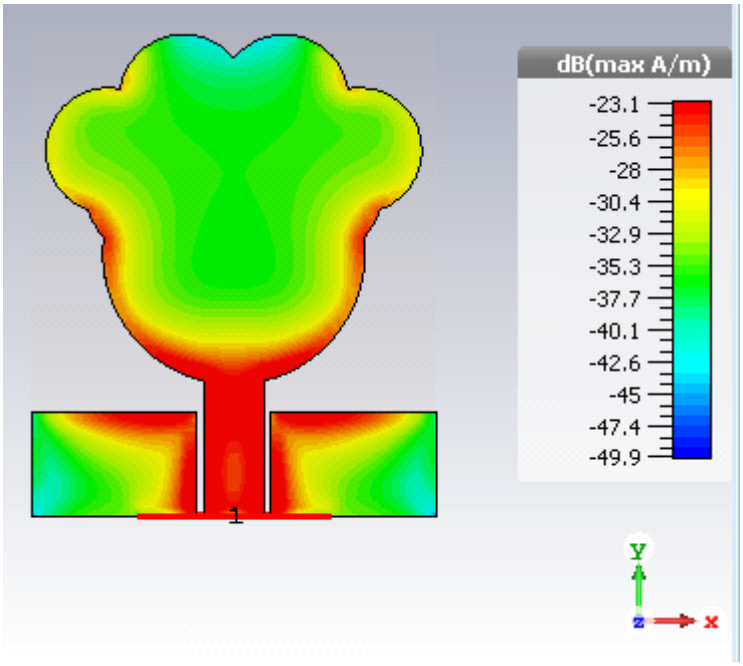

Figure 2.14 Current density distribution at 8.1 GHz

- **Radiation pattern**

Figures 2.15 and **2.16** show the 2D farfield radiation patterns at the frequency 3.45 GHz in the E- (φ=90°) and H- (φ=0°) planes respectively.

Figure 2.15 shows that the pattern in the E-plane consists closely of two lobes, in the two hemispheres. The main lobe exhibits a relatively higher directivity of 4.86 dBi in the maximum direction of propagation θ=156°.

In the H-plane, two lobes are observed in the main directions of propagation with a maximum directivity level of 2.78 dBi in the direction θ=180°.

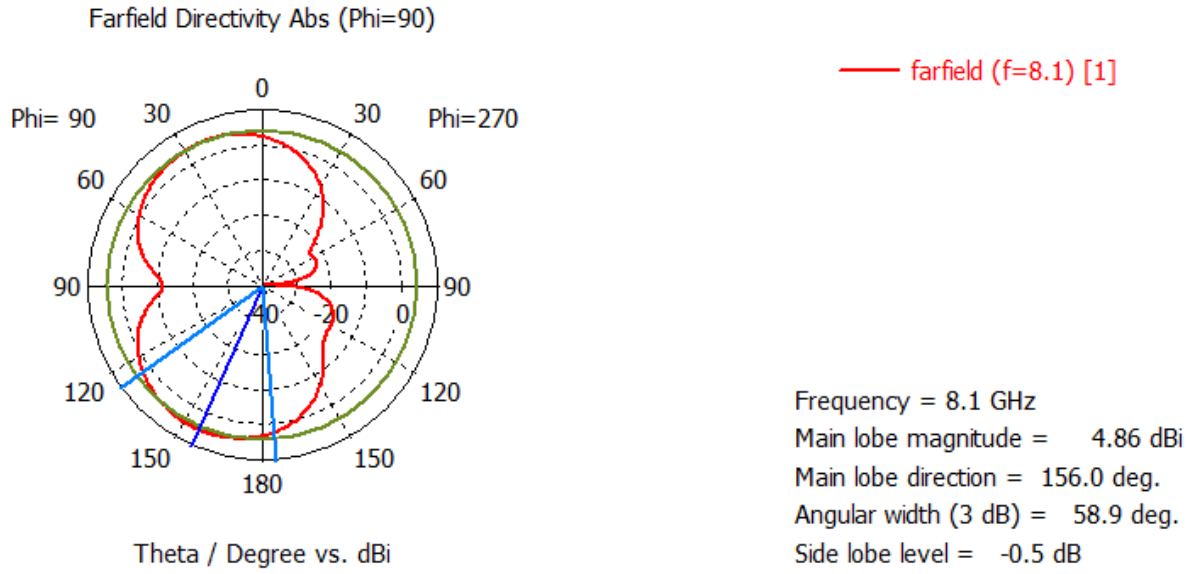

Figure 2.15 Radiation pattern in E-plane at 8.1 GHz

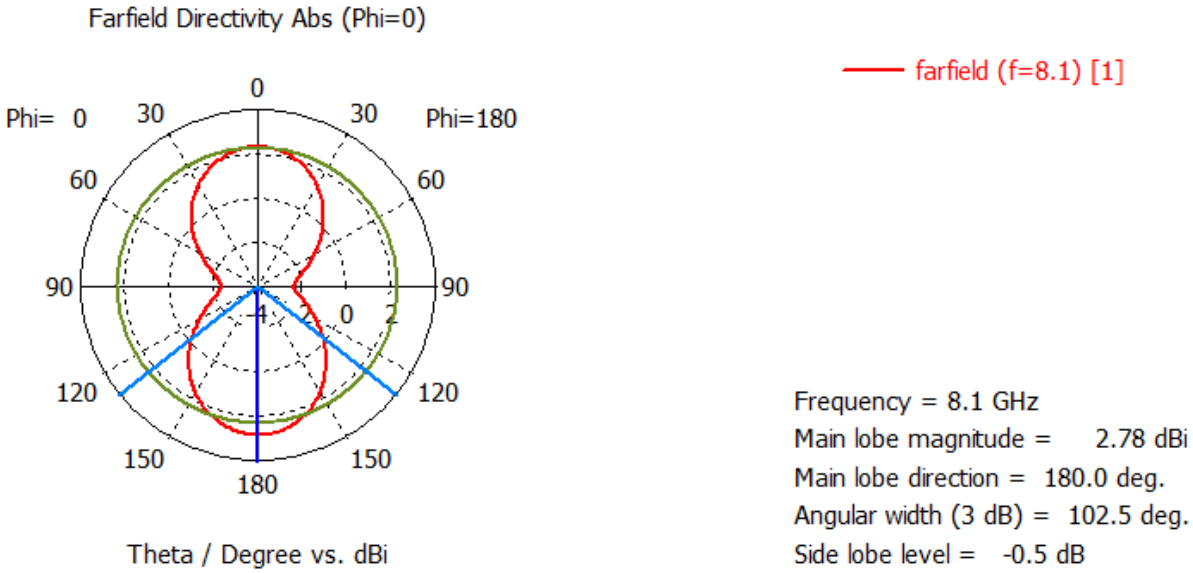

Figure 2.16 Radiation pattern in H-plane at 8.1 GHz

2.3 Conclusion

Throughout this chapter, a fractal UWB coplanar antenna has been developed. The performed two iterations have resulted in an enhanced percent bandwidth of more than 106%. The monopole antenna can be used for the several applications whose operating frequencies are within the obtained bandwidth.

The current density distributions and radiation patterns are simulated at three frequencies located in different parts of the frequency bandwidth. The simulations have shown

qualitative radiation patterns consisting of mainly two lobes in the upper and lower hemispheres respectively.

In the next chapter, reconfigurable slots will be introduced to the last configuration to generate reconfigurable notches.

Chapter 3

Reconfigurable UWB Antenna with Reconfigurable Notches

In this chapter, two slots on the patch and two on the ground plane are added on the developed fractal UWB antenna along with switches that can take ON or OFF positions to open or short the U-shaped slots. The slots will help to bypass (or cut) and/or pass bands of frequencies. The patch antenna is hence able to present reconfigurable frequency notches by suppressing frequency bands according to the switch positions.

The antenna was then implemented and tested to see the match with the simulated results.

3.1 Introducing Slots to the Antenna

This first step consists of introducing slots to the antenna (no switches, equivalent to switches in open positions) to reject widely used frequency bands that might cause interferences to a system using the developed antenna. These frequencies correspond to WLAN (5.2 GHz), WIMAX (6.8 GHz) and in the X-band (8.1 GHz). It is done by etching the copper material on the patch and the ground plane. Four slots have been added, as shown in **Figure 3.1**.

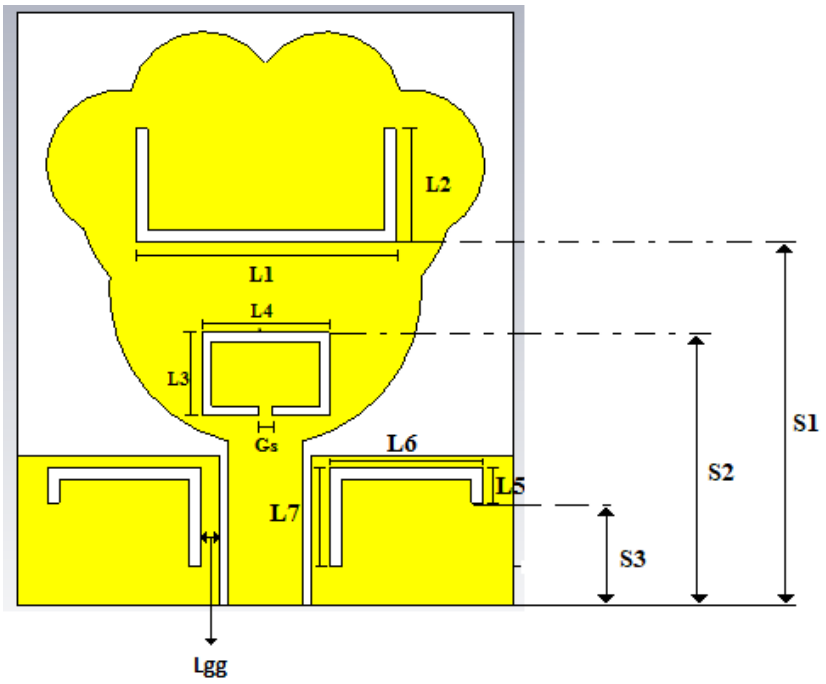

Figure 3.1 Slots dimensions and positions.

The modification consists of a U-shaped slot in the upper side of the patch, a rectangular one below it and two L-shaped slots on the ground plane. These slots (with 0.5 mm thickness) will produce a modification to the original antenna band characteristics that consists mainly on notches that remove frequency bands from the original structure operating bandwidth. The slot length L_{notch} is related to the suppressed frequency wavelength, λg by [27]

$$L_{notch} = \frac{c}{2f_{notch}\sqrt{\varepsilon_{eff}}} = \frac{\lambda_g}{2} \qquad (3.1)$$

Where c denotes the speed of light, f_{notch} the notch frequency and ε_{eff} the medium effective permittivity.

However, this model is not accurate and various parameters need to be fixed usually by simulations such as the slot shape and position. Consequently, several simulations have been carried out inspiring from [5] to end up with a suitable symmetrical configuration that removes the undesired frequency bands. **Tables 3.1** shows the structure slots dimensions and positions.

Table 3.1 Geometrical parameters of the slotted Antenna

Parameter	Value (mm)
L1	10.30
L2	4.30
S1	14.9
L3	3.50
L4	5.40
Gs	1.60
S2	10.8
L5	1.50
L6	5.90
L7	4.20
S3	3.75
Lgg	0.8

3.1.1 Input reflection coefficient

Figure 3.2 shows the slotted antenna input reflection coefficient. It can be seen that the frequency bands involving the undesired frequencies are rejected from the previous band. Again, note that switches have not been added in this simulation.

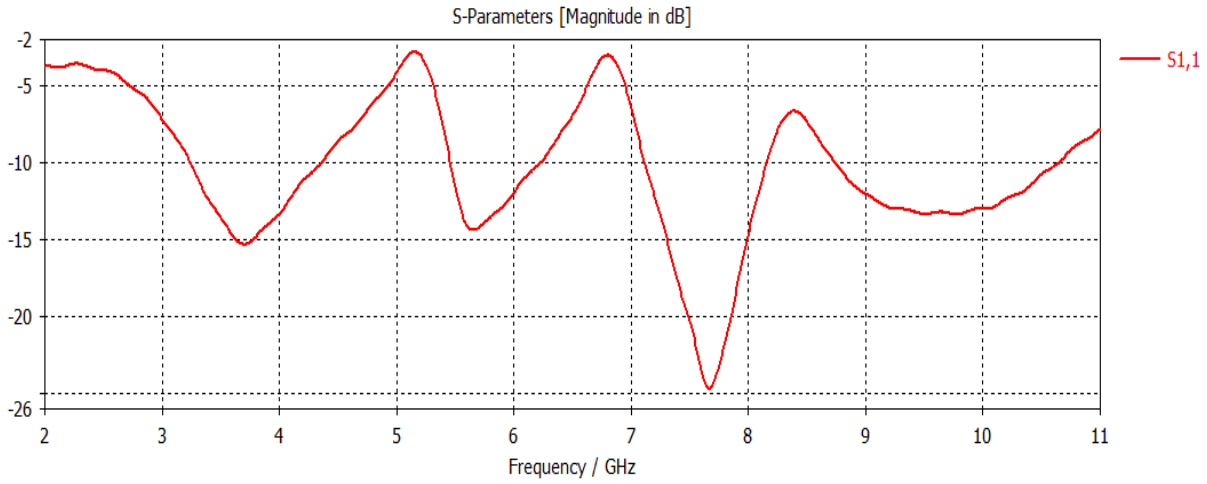

Figure 3.2 Input reflection coefficient of the patch antenna with slots

In what follows, current density distributions and 2D radiation patterns are simulated at the frequencies 3.8 GHz and 5.5 GHz which exhibit lower input reflection coefficient levels in **Figure 3.2** above.

3.1.2 Current Distribution

Figure 3.3 shows the current distribution on the patch with slots at the frequency 3.8 GHz. It can be clearly seen that the current is concentrated at the feedline and at the boundaries of each slot. Also, the current density is too weak in the upper side and in the center of the U shaped slot.

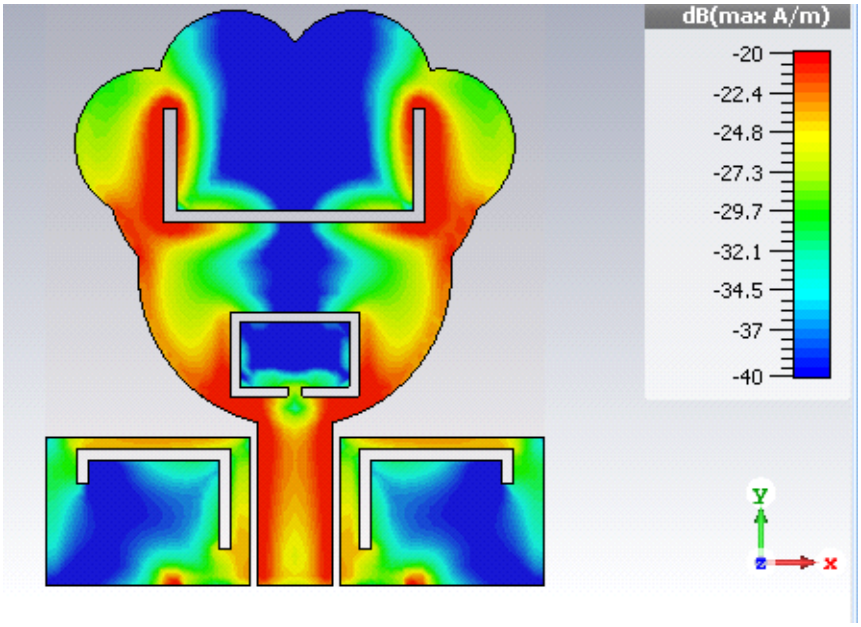

Figure 3.3 Current density distribution at 3.8 GHz.

Figure 3.4 shows the current distribution on the patch antenna with slots at the frequency 5.5 GHz. It is observed from this figure that the current is more concentrated at the feed line and at the boundaries of each slot especially at the upper U shaped slot. Moreover, the current is too weak in the upper edge of the patch and also below the L shaped slots, but comparing it to the 3.8 GHz the current flow is much better than it.

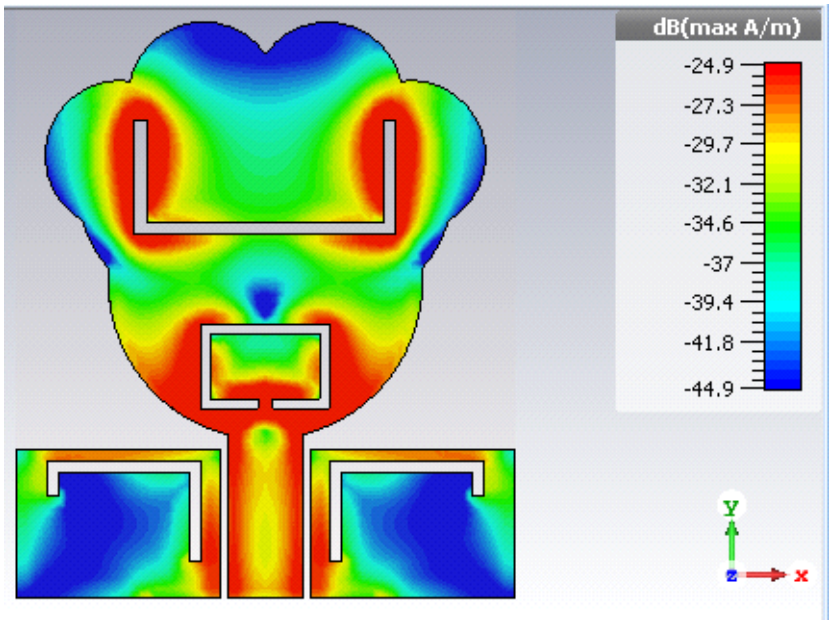

Figure 3.4 Current distribution of the antenna at 5.5 GHz.

3.1.3 Radiation pattern

Figures 3.5 and **3.6** show the 2D farfield radiation patterns at the frequency 3.8 GHz in the E- (φ=90°) and H- (φ=0°) plane respectively.

As expected from a coplanar structure, **Figure 3.5** shows that radiation occurs in both hemispheres with two lobes. The main lobe exhibits a maximum directivity of 2.42 dBi in the direction θ=1°.

Similarly, **Figure 3.5** shows almost two lobes in the H-plane, one in the upper and one in the lower hemisphere, with a maximum directivity of 2.42 dBi in the direction θ=0°.

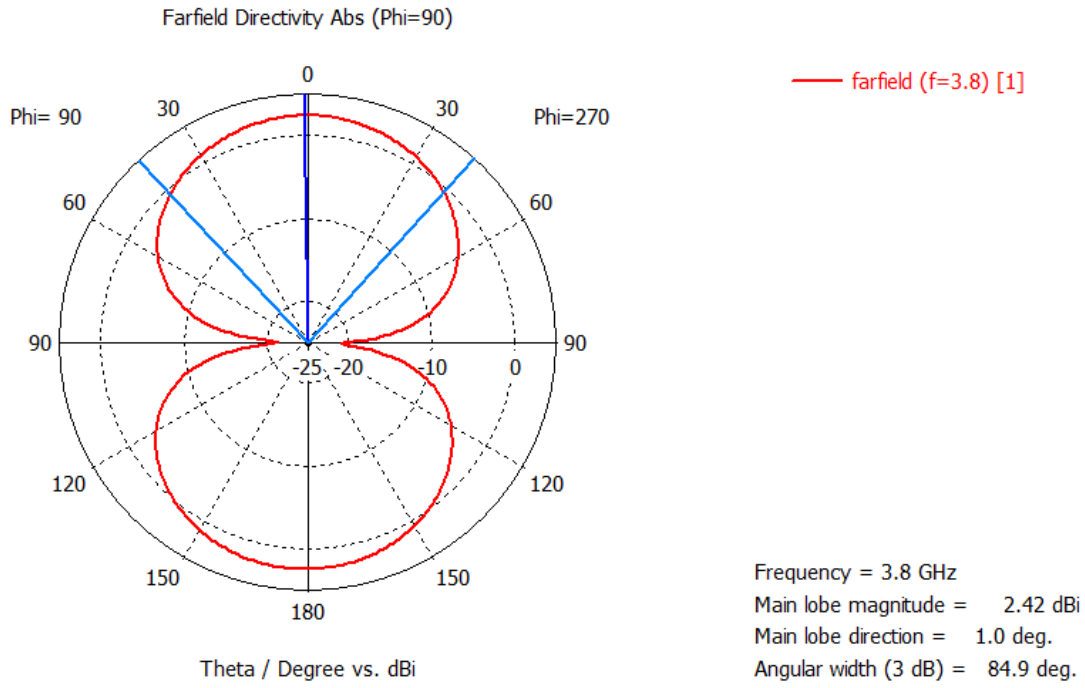

Figure 3.5 Radiation pattern in E-plane at 3.8 GHz

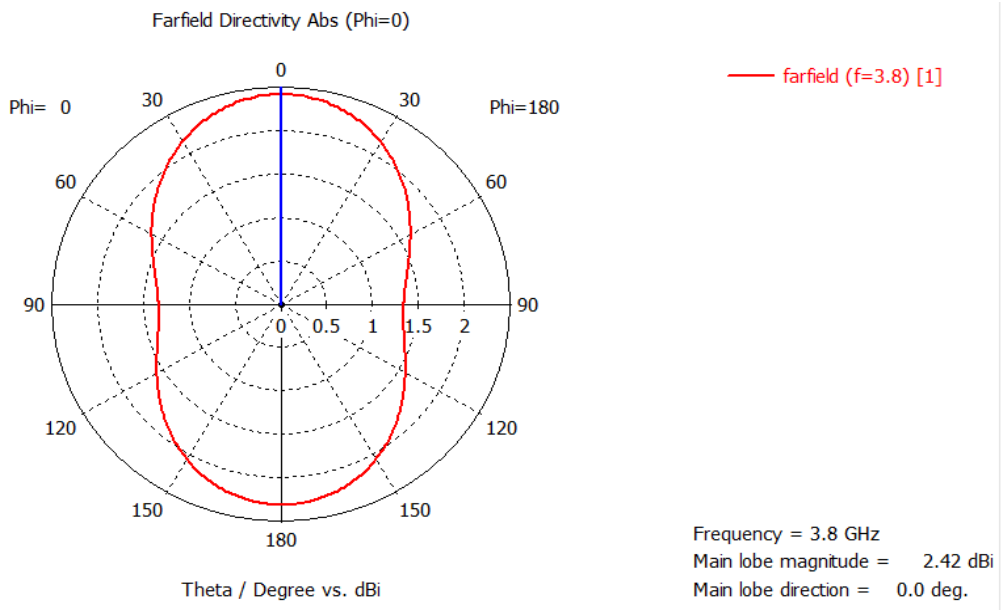

Figure 3.6 Radiation pattern in H-plane at 3.8 GHz

The 2D radiation patterns in the principle planes at the frequency 5.5 GHz are illustrated in **Figures 3.7** and **3.8**.

These figures show almost similar profile in both planes consisting of broad lobes directed to θ=0° and θ=180° respectively. A maximum directivity level of 2.23 dBi is recorded in the direction of θ=0°.

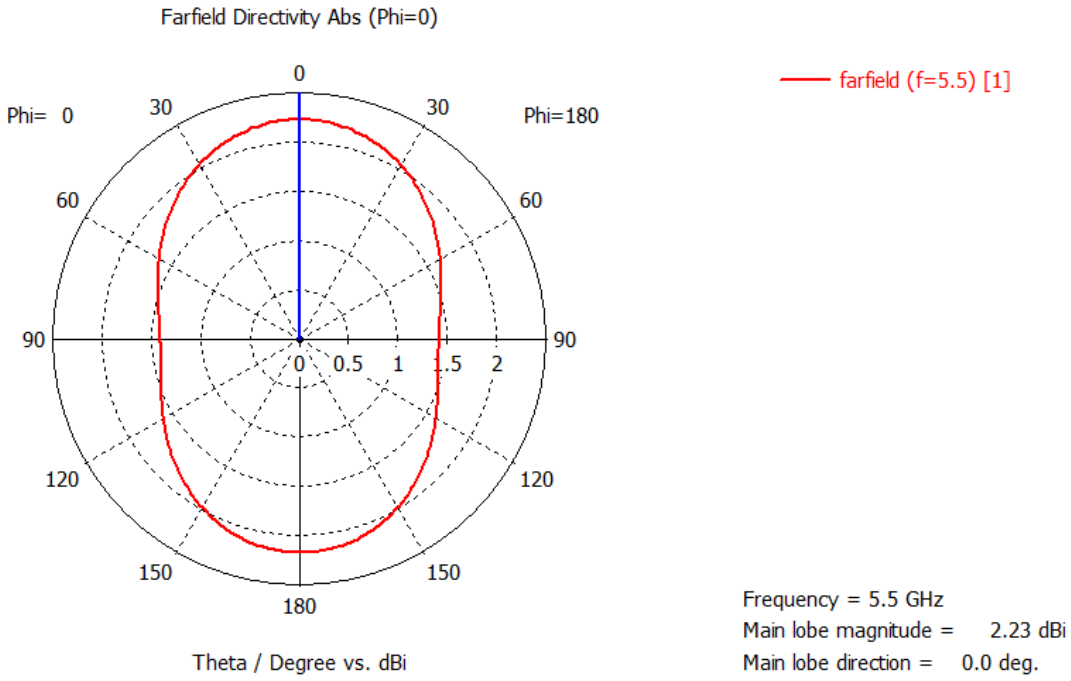

Figure 3.7 Radiation pattern in E-plane at 5.5 GHz

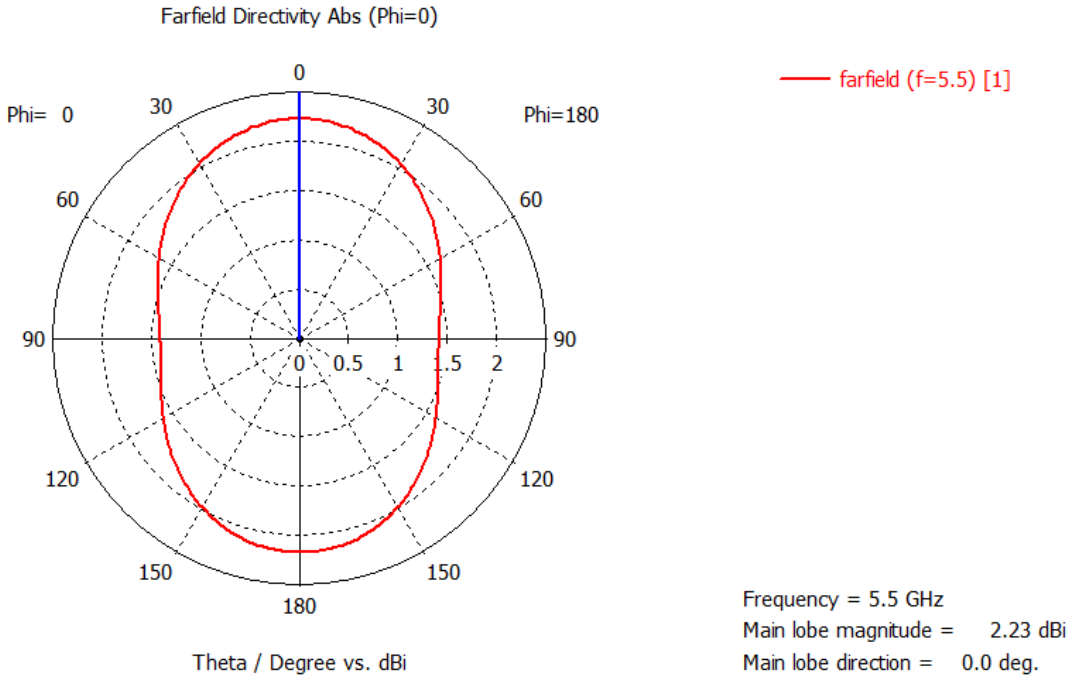

Figure 3.8 Radiation pattern in H-plane at 5.5 GHz

3.2 Introducing switches to the antenna

In this part, two switches are introduced so that the upper U- slot and the lower rectangular slot can be shorted along the antenna axis of symmetry. Consequently, depending on the switch position the slot is shorted if the respective switch is in the 'ON' position and left open if the switch is in 'OFF' position. Accordingly, depending on the positions of the

switches four (4) different antenna configurations and, hence, four (4) operating modes can be obtained achieving notch reconfigurability. These modes are numbered as indicated in **Table 3.2.**

Table 3.2 Switch positions and operating modes

Switches' positions		**Antenna operating mode**
Switch 1 (U-slot)	**Switch 2 (Rectangular slot)**	
OFF	OFF	Mode 1
ON	OFF	Mode 2
OFF	ON	Mode 3
ON	ON	Mode 4

From section 3.1 above where it is noticed that the introduced slots generate frequency bands suppression, shorting and/or leaving the slots open is expected to achieve frequency notch reconfigurability as observed in the following subsections.

Notes:

- Due to the design and implementation complexity of a microwave switch, this part is not considered in the present work where a switch is replaced by a stripline of a width 0.5 mm in the ON state as illustrated in Figures 3.9, 3.11 and 3.13.
- The input reflection coefficient in Mode 1 (OFF, OFF) is investigated in section 3.1 above and the following subsections investigate Modes 2, 3 and 4.

3.2.1 Mode 2 (ON, OFF)

The antenna configuration in Mode 2 where the U-slot is shorted is illustrated in **Figure 3.9** where the closed switch is represented by the stripline.

Figure 3.10 illustrates the input reflection coefficient where it is observed that compared to **Figure 3.2** ($|S_{11}|$ dB in Mode 1), shorting the U-slot results in removing the notch at 5.2 GHz. This denotes that the switch on the U-slots controls whether the 5.2 GHz frequency band (WLAN) is rejected or no.

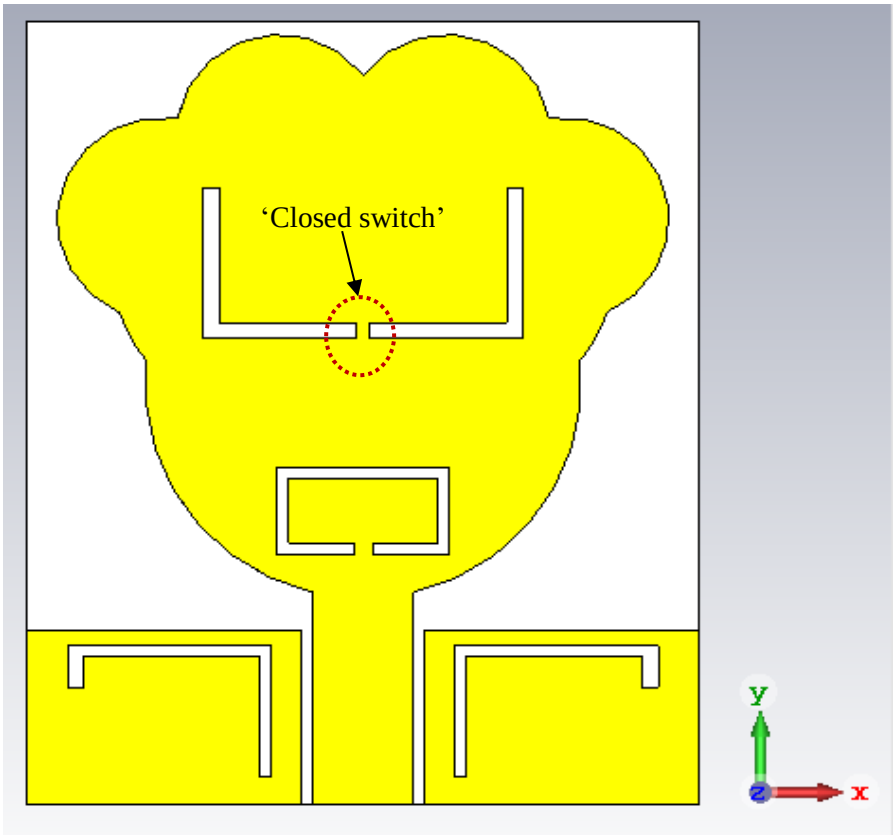

Figure 3.9 Antenna configurations in Mode 2 (ON, OFF)

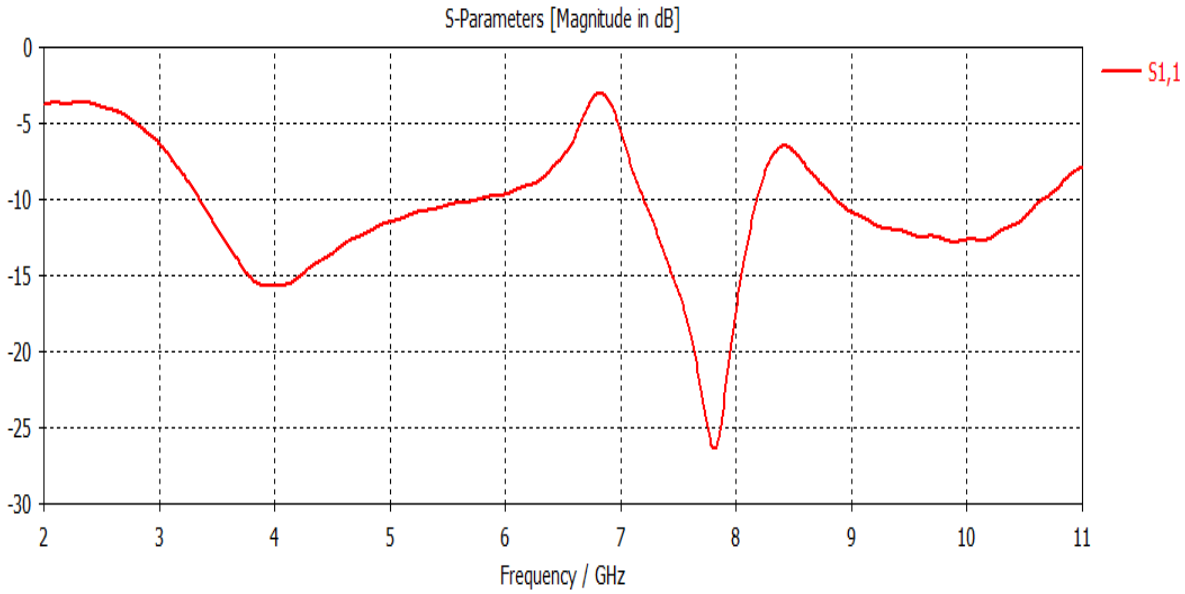

Figure 3.10 Input reflection coefficient in Mode 2 (ON, OFF)

3.2.2 Mode 3 (OFF, ON)

The antenna configuration in Mode 3 where the rectangular slot is shorted is represented in **Figure 3.11**.

The antenna input reflection coefficient in this mode is illustrated in Figure 3.12 where it is

observed that compared to Figure 3.2, the second notch, around 6.8 GHz, is removed denoting that the switch on the rectangular slot controls the presence or not of a notch involving this frequency band (WIMAX).

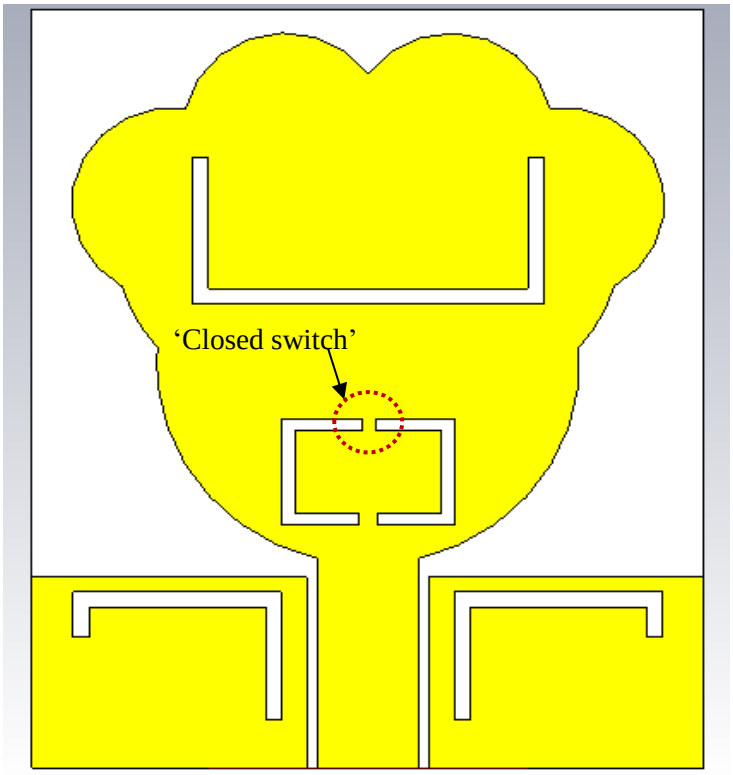

Figure 3.11 Antenna configurations in Mode 3 (OFF, ON)

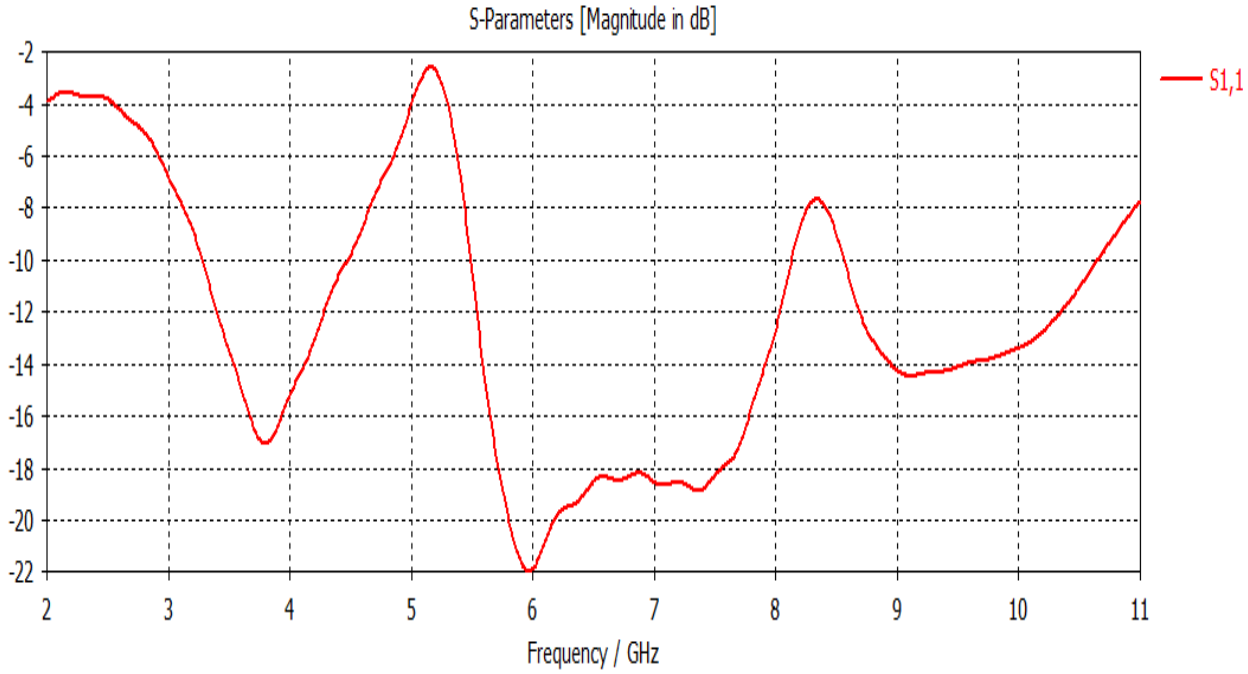

Figure 3.12 Input reflection coefficient in Mode 2 (ON, OFF)

3.2.3 Mode 4 (ON, ON)

The antenna configuration in Mode 4 where both U- and rectangular slots are shorted is illustrated in in **Figure 3.13**.

The input reflection coefficient illustrated in **Figure 3.14** shows that, compared to **Figure 3.2,** notches around 5.2 GHz and 6.8 GHz are removed. This confirms that the switches on the U- and on the rectangular slots control the presence or not of the notches involving the frequency bands around 5.2 GHz (WLAN) and 6.8 GHz (WIMAX) respectively.

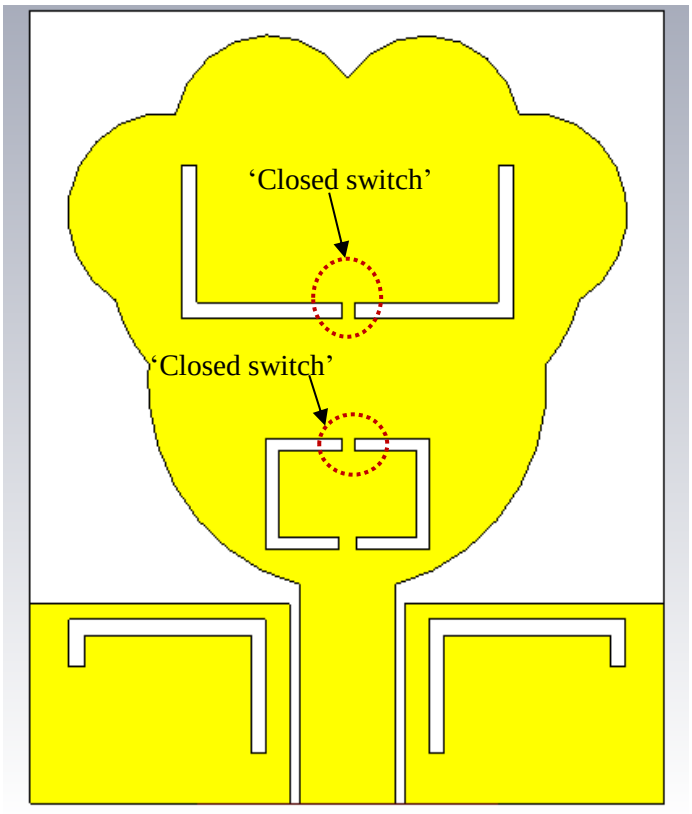

Figure 3.13 Antenna configurations in Mode 4 (ON, ON)

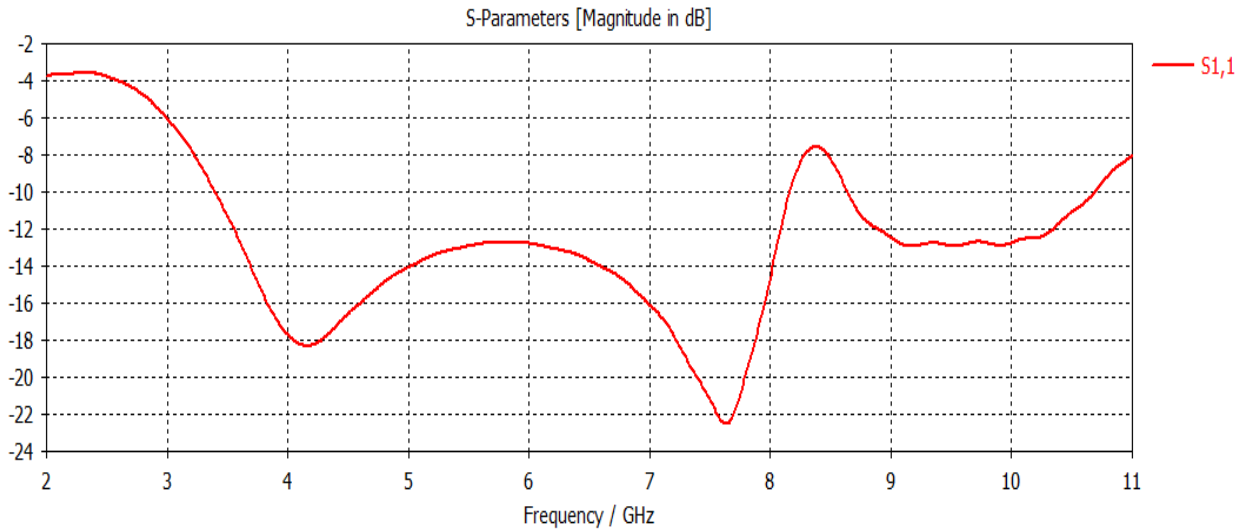

Figure 3.14: S11 of the antenna when both switches are "on"

Finally, **Table 3.3** below summarizes the antenna reconfigurability as it specifies the notched band(s) for each operating mode. It also shows that switches on the U- and on the rectangular slots control rejection of the 5.2 GHz and 6.8 GHz respectively.

Table 3.3 Operating modes and notched bands

Operating Mode / Switches' positions	**Notched band(s)**	
	5.2 GHz	**6.8 GHz**
Mode 1 (OFF, OFF)	Yes	Yes
Mode 2 (ON, OFF)	No	Yes
Mode 3 (OFF, ON)	Yes	No
Mode 4 (ON, ON)	No	No

Simulations have also shown that the notch around 8.1 GHz in the X-band (Figure 3.2) is fixed by the L-shaped slots on the ground plane.

3.3 Experimental results

A prototype of the antenna in Mode 1 (OFF, OFF) configuration is fabricated and its input reflection coefficient measured. **Figures 3.15** shows photographs of the fabricated structure. **Figure 3.16** shows that the simulated and the measured input reflection coefficients have a quite similar profile especially in the C band (4-8 GHz). The observed shifts are attributed to the fact the physical parameters and the geometrical dimensions are not exactly equal to the ones assumed in simulation, fabrication errors and to experimental environment.

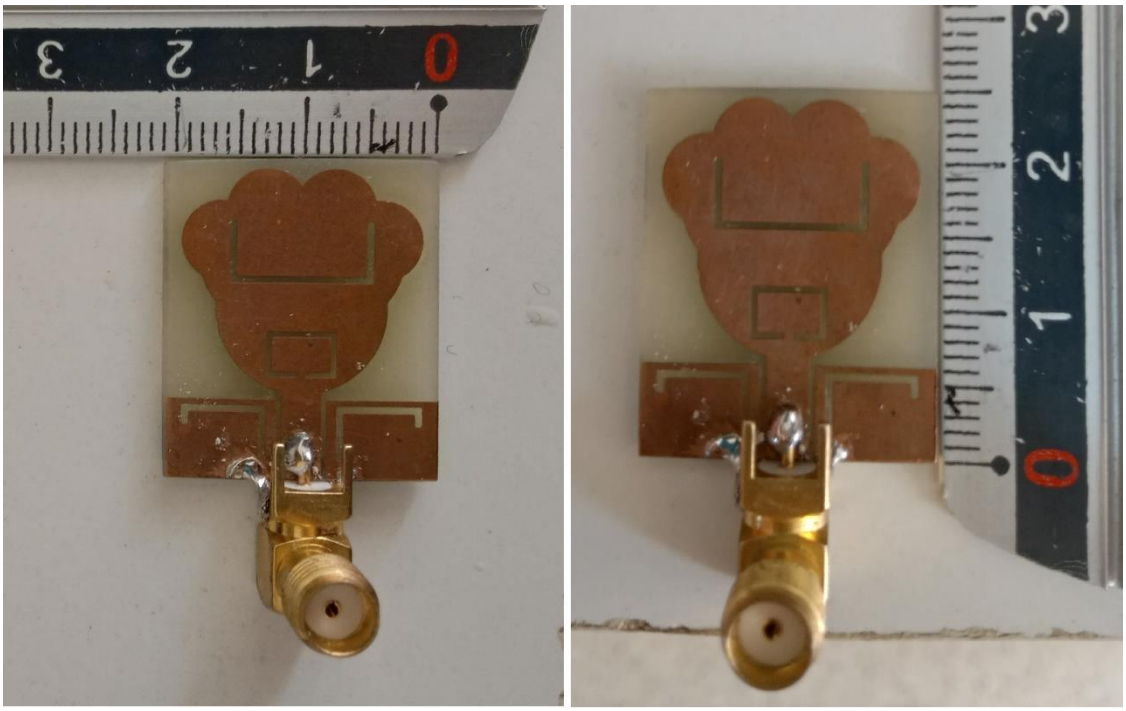

Figure 3.15 Fabricated antenna prototype

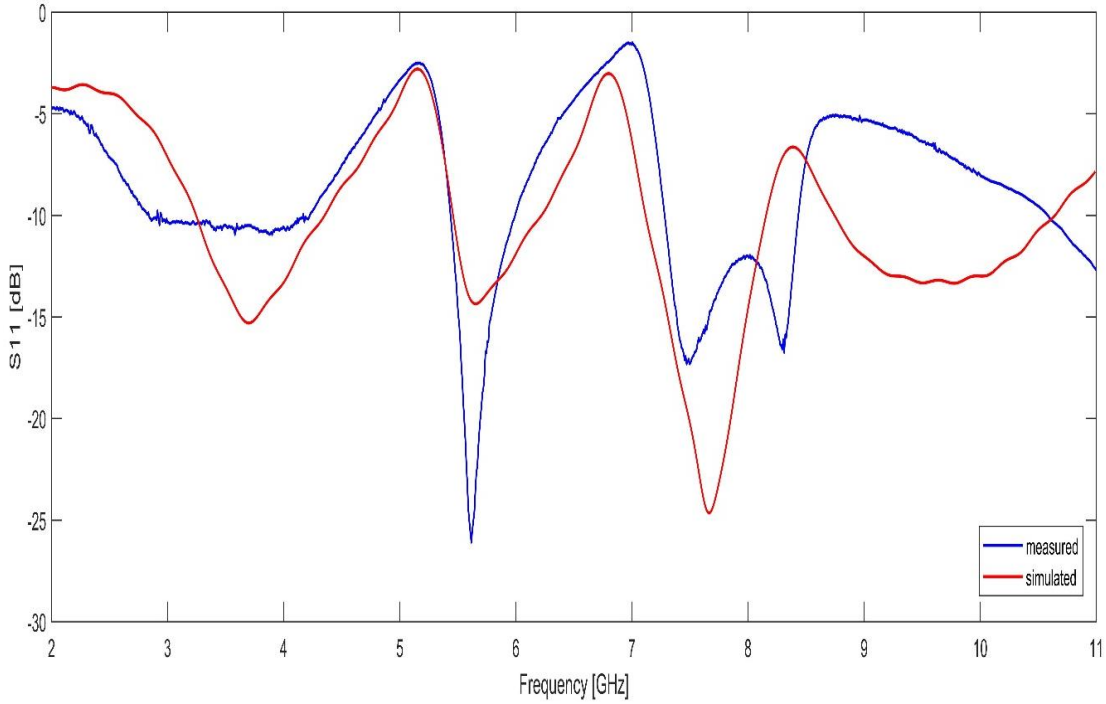

Figure 3.16 Measured versus simulated input reflection coefficient

3.4 Conclusion

In this chapter, three slots are added to the circular fractal antenna which resulted in band notches around 5.2 GHz, 6.8 GHz and 8.1 GHz.

Switches are also added to make it possible to short two slots where it is observed that these switches can control the notches around 5.2 and 6.8 GHz. This allows the antenna to operate in four reconfigurable modes.

The antenna configuration in Mode 1 (OFF, OFF) has been fabricated and tested where quite acceptable results have been obtained.

General Conclusion

Throughout this work, a fractal UWB coplanar antenna has been developed. The performed two fractal iterations have resulted in an enhanced percent bandwidth of more than 106%. The monopole antenna can be used for the several applications whose operating frequencies are within the obtained bandwidth.

In the second part, three slots are added to the circular fractal antenna which resulted in band notches around 5.2 GHz, 6.8 GHz and 8.1 GHz. After that, switches have been added to make it possible to short two slots where it is observed that these switches can control the notches around 5.2 GHz and 6.8 GHz. This allows the antenna to operate in four reconfigurable modes.

The performed simulations using CST software have concerned input reflection coefficient, current density distribution and radiation pattern.

The final antenna configuration, operating in Mode 1 (OFF, OFF), has been fabricated and tested where quite acceptable results have been obtained.

As a further scope, we suggest to perform the following tasks:

- Design and implementation of the switching microwave circuit based on different techniques (PIN diodes, RLC switch)
- Notches' central frequencies and bandwidths tuning.

References

[1] Patel, B, D. Microstrip Patch Ante nna-A Historical Pe rspe ctive of the Developme nt. india : Atlantis Press, 2013, Vol. p. 445-449.

[2] Balanis. s.l. : Hoboken, Antenna theory: analysis and design. Constantine, A et 2005. 047166782X.

[3] P. Bhartia, I. Bahl. s.l.: Artech House, Microstrip Antenna Design Handbook. 2000.

[4] Bernhard., J.T. s.l. Reconfigurable Antennas. : Synthesis Lectures on Antennas, 2007.

[5] A. Falahati, Amir H. Nazeri, Robert Edwards A Novel Compact Fractal UWB Antenna with Triple Reconfigurable Notch Reject Bands Application.. s.l. : AEU - International Journal of Electronics and Communications 101, 2019.

[6] Bernhard, G.H. Huff and J.T. s.l. : C.A. Balanis, 2008, Vol. Modern Antenna Handbook. John Wiley & Sons.

[7] C.J., Chauraya, A. et Vardaxoglou, J.C. s.l. Frequency and beam reconfigurable antenna using photoconducting switches. Panagamuwa, : IEEE Trans. Antennas Propag, 2006. 2006ITAP...54..449P. doi:10.1109/TAP.2005.863393. S2CID 8074147..

[8] Erdil, E, et al. s.l. Frequency tunable microstrip patch antenna using RF MEMS technology.: IEEE Trans. Antennas Propag., 2007. 2007ITAP...55.1193E. doi:10.1109/TAP.2007.893426. S2CID 19335959.

[9] X.S., Yang, et al. s.l. Yagi Patch Antenna With Dual-Band and Pattern Reconfigurable Characteristics.: IEEE Antennas Wirel. Propag., 2007. 7752473..

[10] MEMS reconfigurable vee antenna. Chiao, J.C., et al. s.l. : IEEE MTT-S International Microwave Symposium, 1999. 10.1109/MWSYM.1999.780242. ISBN 978-0-7803-5135-6. S2CID 7946482.

[11] Rodrigo, D., Jofre, L. et Cetiner, B.A. s.l. Circular Beam-Steering Reconfigurable Antenna With Liquid Metal Parasitics.: IEEE Trans. Antennas Propag, 2012:10.1109/TAP.2012.2186235. S2CID 36089245.

[12] Aboufoul, T., et al. s.l. Pattern-Reconfigurable Planar Circular Ultra-Wideband Monopole Antenna: IEEE Trans. Antennas Propag. , 2013. 10.1109/TAP.2013.2274262. S2CID 9565138.

[13] Harrington, R.F. s.l. Reactively controlled directive arrays: IEEE Trans. Antennas Propag, 1978. 10.1109/TAP.1978.1141852..

[14] Hum, S.V. et Perruisseau-Carrier, J. s.l. Reconfigurable Reflect arrays and Array Lenses for Dynamic Antenna Beam Control: A Review: IEEE Trans. Antennas Propag, 2014. 10.1109/TAP.2013.2287296. S2.

[15] Simons, R.N., Donghoon, C. et Katehi, L.P.B. s.l Polarization reconfigurable patch antenna using microelectromechanical systems (MEMS) actuators.. : IEEE Antennas Propag., 2002. 978-0-7803-7330-3..

[16] Liu, L. et Langley, R. s.l. Liquid crystal tunable microstrip patch antenna.: Electronics Letters, 2008. 2008ElL....44.1179L. doi:10.1049/el:20081995..

[17] Aboufoul, T., et al. s.l.Multiple-parameter reconfiguration in a single planar ultra-wideband antenna for advanced wireless communication systems. : IET Microwaves, Antennas & Propagation, 2014. 849–857.

[18] Rodrigo, D., Cetiner, B.A. et Jofre, L. s.l.Frequency, Radiation Pattern and Polarization Reconfigurable Antenna Using a Parasitic Pixel Layer. : IEEE Trans. Antennas Propag, 2014. 2014.2314464.

[19] Pringle, L.N. et al., et. s.l. A reconfigurable aperture antenna based on switched links between electrically small metallic patches.: IEEE Trans. Antennas Propag., 2004. 25035434.

[20] G.E. Ponchak, J.PApapolymerou, and M. M. Tentzeris. 8, s.l.S. Nikolaou, N.D. Kingsley UWB elliptical., : IEEE Trans., 2009, Vol. 57.

[21] Motovilova, Elizaveta et Huang, Shao Ying. s.l. A Review on Reconfigurable Liquid Dielectric Antennas.: Materials (Basel, Switzerland), 2020. 32316173.

[22] C. G. Christodoulou, Y. T. Tawk, S. A. Lane, and S. R. 7, s.l. Reconfigurable antennas for wireless and space applications.: IEEE Proc. , 2012, Vol. 100.

[3] Pozar, D. M. Microstrip Antenna. 1, s.l.: IEEE, 1992, Vol. 80.

[23] H. Jiang, M. Pattersons.l, C. Zhang, and G. Subramanyam,. Frequency agile microstrip patch antenna using ferroelectric thin film varactor technology.. : in Proc. IEEE Antennas Propag. Soc. Int. Symp, 2009.

[24] S. W. Cheung and T. I. Yuk,. 6, s.l H. L. Zhu, X. H. Liu Design of polarization reconfigurable antenna using metasurface.,. : IEEE Trans. Antennas and Propag. , 2014,Vol. 62.

[26] ,. E. Erdil, K. Topalli, M. Frequency tunable patch antenna using RF MEMs technology,.. Unlu, O.A. Civi, and T. Akin,. 4, s.l. : IEEE Trans. Antennas Propag, 2009, Vol. 55.

[27] D. M. Pozar, "Microwave engineering," ed: John wiley & sons, 2011.